DIPLOMA THESIS

Cardiac and baroreflex responses: from tilt table to gated auricular Vagus Nerve Stimulation

carried out for the purpose of obtaining the degree of

Dipl. Ing.

in

Biomedical Engineering

by

Andreas Dickinger, BSc

0826852

under the supervision of

Dipl.-Ing. Dr.techn. Babak Dabiri

Univ.Prof. Dipl.-Ing. Dr.techn. Eugenijus Kaniusas

Institute of Biomedical Electronics

2023

Acknowledgments

Firstly I would like to thank my supervisor, Dipl.-Ing. Dr.techn. Babak Dabiri, for making this thesis possible. Always patient and despite working hard on his own diploma, he always found the time to be helpful when I needed him.

Secondly, I would also like to thank Ao. Univ. Prof. Dipl.Ing. Dr.techn. Eugenijus Kaniusas for the valuable opportunity to finish my thesis here, at Institute of Biomedical Electronics. Despite always being busy, he never failed to give advice and help out when students needed him.

Thirdly, I want to thank my sister Elisabeth for helping me out during the experiments conducted in this thesis. She volunteered a significant amount of her time to help me achieve this masters degree, for that I will be forever grateful.

I also wish to express my deepest gratitude to my mother Christine for supporting me during my studies.

Finally, I want to thank my fellow students and friends, who have to remain anonymous, for participating in the experiments.

.

ABSTRACT

The variability of the heart rate and its response to external stimuli has long been of clinical importance. Recently the cardiovagal baroreflex sensitivity *BRS* has been investigated as an additional diagnostic tool for a number of diseases. Traditionally *BRS* was estimated using linear regression, a more recent method uses a best fit ellipse approximation.

Auricular vagus nerve stimulation (aVNS) is a non-invasive neuromodulatory therapy for a number of chronic illnesses. To achieve a more individualized treatment closed-loop aVNS systems, synchronised to patients vital signals, are being developed and tested.

In this work two different sets of experiments were conducted to investigate the effects of external stimuli on the human cardiovascular system. Firstly the *BRS* was investigated in various head up tilt body positions, from supine, 30°, 60°, 80° head up tilt to the standing position. Seven subjects voluntarily participated and slow paced breathing was employed throughout to exaggerate heart rate variability and the baroreflex. The results were searched for continuous sequences of rising and falling heart rate variability *RR* and systolic blood pressure P_S, representing the cardiovagal baroreflex, then analysed using both a best fit ellipse method and linear regression.

The second experiment investigated the effect of synchronised auricular vagus nerve stimulation. Measurements were conducted following two different protocols, the first using cardiac gated aVNS, the second respiratory gated aVNS. Five subjects volunteered, with each subject participating twice for a total of 10 measurements per protocol. The recorded blood pressure and ECG data was analysed in both time and frequency domain.

The results show significant differences in the estimated *BRS* between different head up tilt positions. The ellipse method resulted in median values of 28, 19.8, 11.9, 11.5 and 11.2 ms/mmHg for supine, 30°, 60°, 80° and standing, a mirrored trend also seen in the linear regression. A detailed beat by beat analysis also confirmed a lower *BRS* for the more upright positions, with significantly higher *BRS* changes recorded during expiration than inspiration and thereby confirming the baroreflex hysteresis. Of the aVNS experiments only the respiratory gated experiment recorded any significant changes. Here the inspiration synced aVNS showed an increasing trend in the root mean square of successive differences between normal heartbeats *RMSSD* over the non aVNS baseline, indicating an increased high frequency content in the heart rate variability. Additionally the respiration rate dropped for both inspiratory and expiratory synchronised aVNS.

Overall the head up tilt experiment provided new insight into *BRS* response, the resulting estimates comparable to other studies. While the aVNS experiments were likely too short for significant results, the trends in the respiration gated aVNS do show promise for further study.

ZUSAMMENFASSUNG

Die Variabilität der Herzfrequenz und ihrer Reaktion auf äußere Reize ist seit langem von klinischer Bedeutung. Vor kurzem wurde die kardiovagale Baroreflexsensitivität *BRS* als zusätzliches diagnostisches Instrument für eine Reihe von Krankheiten untersucht. Traditionell wurden *BRS* Schätzungen mit linearer Regression berechnet, eine neuere Methode verwendet allerdings eine Best-Fit-Ellipse.

Aurikuläre Vagusnervstimulation (aVNS) ist eine nicht-invasive neuromodulatorische Therapie für eine Reihe von chronischen Krankheiten und Störungen. Um eine individualisierte Behandlung zu erreichen, wurden Closed-Loop-aVNS-Systeme entwickelt, die auf die Biosignale des Patienten abgestimmt sind.

In dieser Arbeit wurden zwei verschiedene Versuchsreihen durchgeführt, um die Auswirkungen externer Stimuli auf das menschliche Herz-Kreislauf-System zu untersuchen. Zuerst wurde die *BRS* in verschiedenen Kopf nach oben geneigten Körperpositionen von Rückenlage, 30°, 60°, 80° Kopfneigung bis zum Stehen untersucht. Sieben Probanden nahmen freiwillig teil, wobei verlangsamte Atmung eingesetzt wurde, um die Herzfrequenzvariabilität und den Baroreflex zu übertreiben. Die Ergebnisse wurden nach kontinuierlichen Sequenzen von ansteigenden und fallenden RR und P_S, die das Herz-Kreislauf-System repräsentieren, durchsucht und dann mittels linearer Regression und einer Best-Fit-Ellipse-Methode analysiert.

Das zweite Experiment untersuchte die Wirkung einer synchronisierten Aurikular-Vagus-Nerv-Stimulation (aVNS). Die Messungen wurden anhand zwei verschiedener Protokolle durchgeführt, das erste mit herzgesteuertem aVNS, das zweite atmungsgesteuertem aVNS. Fünf Probanden meldeten sich freiwillig, wobei jeder Proband zweimal für insgesamt 10 Messungen pro Protokoll teilnimmt. Die aufgezeichneten Blutdruck- und EKG-Daten wurden sowohl im Zeit- als auch im Frequenzbereich analysiert.

Die Ergebnisse zeigen signifikante Unterschiede in der geschätzten *BRS* zwischen verschiedenen Neigungspositionen. Die Ellipsenmethode ergab Medianwerte von 28, 19,8, 11,9, 11,5 und 11,2 ms/mmHg für Rückenlage, 30°, 60°, 80° und Stehen ein Trend, der auch in den Werten der linearen Regression zu sehen ist. Eine detaillierte Schlag-für-Schlag-Analyse ergab auch eine niedrigere *BRS* für die aufrechteren Positionen, wobei signifikant höhere *BRS*-Änderungen innerhalb der Ausatmungsphase als während der Einatmung aufgezeichnet wurden, und somit die Baroreflex-Hysterese bestätigte wurde.

Von den aVNS-Experimenten verzeichnete nur das Atmungsgesteuerte signifikante Veränderungen. Hier zeigte das Einatmungs synchronisierte aVNS einen steigenden Trend bei

dem quadratischer Mittelwert der Differenzen aufeinanderfolgender R-R-Intervalle *RMSSD* gegenüber der Basislinie ohne aVNS, was auf einen höheren Hochfrequenzanteil (HF) der Herzratenvariabilität hinweist. Zusätzlich verringerte sich die Atemfrequenz sowohl bei dem Ein- und Ausatmungs synchronisiertem aVNS.

Insgesamt lieferte das Neigungsexperiment neue Einblicke in die *BRS*, wobei die resultierenden Schätzungen mit anderen Studien vergleichbar waren. Während die aVNS-Experimente wahrscheinlich zu kurz waren,um signifikante Ergebnisse zu erzielen, sind die Trends beim Atmungsgesteuertem aVNS vielversprechend.

Contents

List of Abbreviations and Variables

ANS	.....	autonomic nervous system
AV	.....	atrioventricular valves
aVN	.....	auricular vagus nerve
aVNS	.....	auricular vagus nerve stimulation
BRS	.....	cardiovagal baroreflex sensitivity
CBC	.....	cardiovagal baroreflex cycle
ECG	.....	electrocardiogram
f_C	.....	value of heart period
f_R	.....	respitation frequency
HF	.....	high frequency
HR	.....	heart rate
HRV	.....	heart rate variability
IQR	.....	interquartile range
LF	.....	low frequency
P_D	.....	diastolic blood pressure
P_S	.....	systolic blood pressure
PNS	.....	parasympathetic nervous system
PPG	.....	photoplethysmogram
RMSSD	.....	Root Mean Square of Successive Differences
RR	.....	inter beat interval from electrocardiogram
SA	.....	sinoatrial
SDNN	.....	Standard Deviation of the NN Interval
SL	.....	semilunar valves
SNS	.....	sympathetic nervous system

List of Tables

List of Figures

Chapter 1

Introduction

The heart is the center of the blood circulating system, carriing oxygen and nutrients to the body while removing waste produces like carbon dioxide to the lungs. It also participates in the regulation of blood pressure, primarily through the adjustment of the heart rate, but also the stroke volume (Kaniusas, 2012). The variability of the heart rate and therefore its ability to regulate the blood pressure has long been of clinical importance as a predictor of various illnesses such as acute myocardial infarction (LaRovere et al., 1998) or diabetic neuropathy (Task Force, 1997). The human body has many mechanisms to influence the heat rate variability (HRV), but among the most important is the baroreflex.

The baroreflex is an essential part in maintaining near constant blood pressure. Like the heart it is governed by the autonomic nervous system, and its cardiovagal component is an indicator of the parasympathetic (PNS) and sympathetic (SNS) activities modulating the heart rate (Kaniusas, 2012). The quantification of the baroreflex has therefore been sought after as a diagnostic tool, with studies showing that the cardiovagal baroreflex sensitivity (BRS) may provide prognostic value in heart failure (Benarroch, 2008) and diabetes (Chapleau, 2012).

Experiments conducted to investigate the cardiovagal baroreflex were preformed either as non invasive recordings of spontaneous fluctuations in the cardiac interval RR and systolic blood pressure P_S(O'Leary et al., 2003), or induced blood pressure changes through vasoactive drugs or other external mechanisms (LaRovere et al., 1998). In these experiments the influence of the body position has not yet been thoroughly investigated, with few studies comparing BRS in two different head-up tilt positions (Choi et al., 2006)(Taylor et al., 2013). Until recently the BRS estimates themselves were mainly calculated using linear regression, although a novel method using a best fit ellipse was recently developed (Dabiri et al., 2021).

Electrical stimulation of the auricular vagus nerve (aVNS) is a a novel neuromodulatory therapy used for treatment of various illnesses and disorders such as epilepsy, depression or stroke recovery (Ben-Menachem, 2000)(Sackeim et al., 2005)(Kaniusas et al., 2019a). Currently aVNS treatments are non-individualised, with little regard for the underlying physiological state of the patient, therefore delivering the optimal treatment is difficult. Lately

closed loop aVNS stimulators ahve been developed, that manage to avoid over- and under-stimulation through the use of bio-signal feedback. These new devices are also capable of stimulation synchronised to various physiological processes such as the heartbeat or respiration, enabling potentially new treatment protocols (Kaniusas et al., 2019b).

The goal of this work is to present a investigation into the response of the cardio-vagal system to external stimuli. The first part of this work concerns the changes in the baroreflex in response to postural changes. Here the vital signals of several patients will be recorded in a number of different Head-Up Tilt positions, using a paced breathing method to amplify the baroreflex. These signals will then be analysed for baroreflex sequences and the estimated BRS presented using an elliptical model. The second part of this work concerns experiments using auricular vagus Nerve Stimulation (aVNS). Several measurements are carried out on subject experiencing vagus nerve stimulation, with the stimulation pulses synchronised to either their respiration or their atrial blood pressure waveform.

This work is structured as follows. Chapter 1 provides an overview of the basic concepts discussed in this work, from an introduction to the cardiac cycle, the baroreflex to the principles of auricular vagus nerve stimulation (aVNS). In Chapter 2, the experimental setup for the Head-Tilt and aVNS measurements are described. Furthermore the methods used for evaluating and analysing the data collected from the experiments are also presented. The results of the measurements and their statistical analysis are presented in Chapter 3 and discussed in Chapter 4.

1.1 Vital physiology

This section presents the fundamentals of anatomy, physiology and signal analysis which are relevant to the understanding of this work.

1.1.1 Heartbeat

The heart is the motor for the circulatory system, pumping blood throughout the entire body, transporting nutrients and oxygen to cells, circulating unwanted substances generated during their metabolism to filtration organs, as well as regulating pH and temperature levels. The mechanical contractions of the heart are tightly interrelated with its electric impulses. A full contraction and relaxion cycle of the heart is called a heartbeat, they are initiated and controlled by the sinoatrial node. The process is as follows.

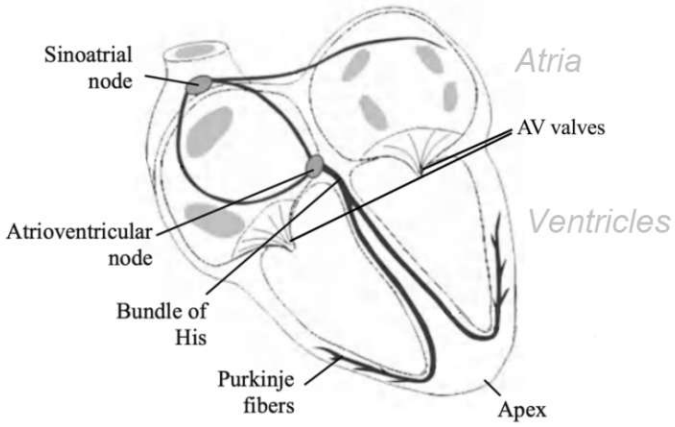

Figure 1·1: An illustration of the heart and its main electrical transmission pathways. Taken and modified from (Malmivuo and Plonsey, 1995).

The electrical depolarization of the heart is initiated by the sinoatrial node (SA) and propagates through fibres on the wall of the atria towards the atrioventricular node (AV), marking the beginning of the atrial systole. At first this causes the atria to contract, forcing a final amount of blood to enter the ventricles through open AV valves. The semilunar (SL) valves that connect the arteries to the ventricles are closed at this point.

Then the action potential reaches the AV node, where after a small delay to ensure the atria have contracted, it is then forwarded down the Bundle of His towards the ventricular Purkinje fibres causing the ventricles to start to contract. The AV valves close and pressure in the ventricle rises until it exceeds the pulmonary and aortic pressure respectively, at which point the SL valves open. This marks the end of the atrial systole and the start of the ventricular systole.

After the valves open the stroke volume, about 2/3 of the heart's blood volume, leaves the heart towards the arteries. Pressure first rises, but then starts to fall as the ventricles start to relax. Blood flow also slows and for a short time turns negative causing the SL valves to close. This backflow causes a short dip in blood pressure known as the dicrotic notch. Ventricular pressure continues to fall further until the dip below arterial pressure and the AV valves open. The ventricles start filling again and the cycle begins anew (Kaniusas, 2012). A graphical representation of the heart is depicted in Figure 1·1.

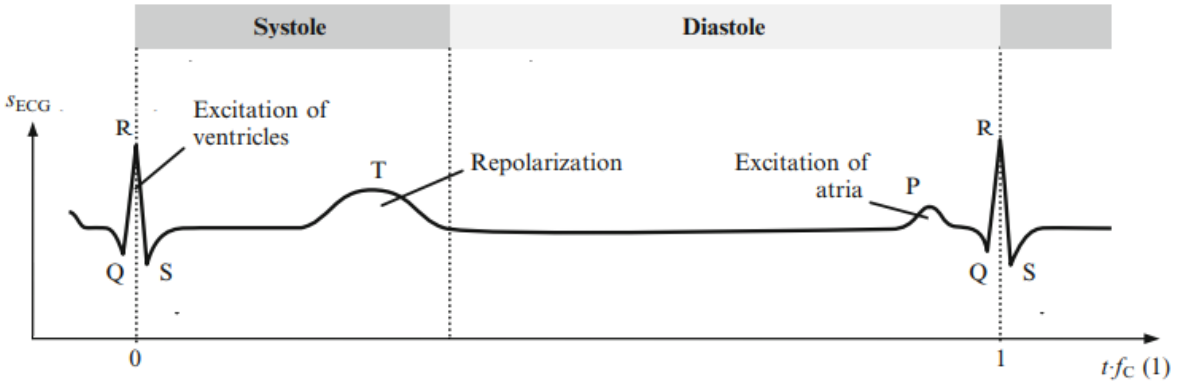

Figure 1·2: An ECG and its main parameters. Taken and modified from (Kaniusas, 2012).

One of the most common ways to register the activity of the heart is through a processes known as an Electrocardiogram (ECG), whereby the electrical activity of the cardiac muscles is recorded. This is done by placing electrodes on the surface of the skin to register the impulses caused by the polarisation and depolarisation of the heart fibres. As can be seen in Figure 1·2, the ECG manages to provide exact timing information about the different stages of the cardiac cycle. It consists of the following segments (Stroobandt et al., 2016).

- P wave: corresponds to the atrial depolarization form the SA node towards the apex of the heart. The wave returns toward the isoelectronic baseline when both atria are fully depolarised.

- QRS complex: corresponds to the moment of depolarization of the ventricles. For a moment the polarisation continues towards the base of the heart, resulting in the Q-wave. The polarisation then starts to turn towards the top of the heart resulting in the large R-peak, then reversing again until the ventricles are completely depolarised leaving behind the S-peak and the isoelectronic baseline.

- T wave: corresponds to ventricular repolarization and at its end, the ventricular systole ends.

The value of heart period, also known as the RR interval, is usually defined as the interval of time between consecutive R peaks, of the ECG, and it corresponds to the inverse of the heart rate (f_C). For accurate RR measurements a sampling rate of at least 500Hz is required (Kaniusas, 2012).

1.1.2 Heart Rate Variability

Heart Rate Variability (HRV) corresponds to the variations in both instantaneous RR and f_C. It is considered a relevant clinical indicator of the integrity of autonomic functions and HRV perturbations are linked to early onset of cardiovascular diseases pathologies, like acute myocardial infarction (LaRovere et al., 1998) or diabetic neuropathy (Task Force, 1997).

HRV can be analysed both in the time domain and the frequency domain. Time domain analysis consist of calculating and comparing statistical values e.g. mean, standard deviation, between measurements or a reference. An analysis in the frequency domain includes fast Fourier transforms and power spectral density calculations. Here the spectrum is divided into four separate frequency bands, ultra-low-frequency (ULF), very low frequency (VLF), low frequency (LF) and high frequency (HF) bands (Shaffer and Ginsberg, 2017).

- The ULF band (0-0.003 Hz) is used to index long term fluctuations with a period of 5 min or longer, generally for measurements exceeding 24h. It primarily reflects circadian variation (Bilgeand et al., 1999).
- The VLF band (0.0033–0.04 Hz) is an indicator sympatho-vagal balance and has been shown to represent influence of the thermoregulatory and renin-angiotensin system. Furthermore the VLF components have a strong association with cardiovascular disease prognosis and metabolic syndrome (Bilgeand et al., 1999).
- The LF band encompasses a band from 0.04 to0.15 Hz. LF power is connected to both the PNS and SNS, but it mainly reflects blood pressure regulation through baroreceptor activity, particularly in resting conditions. Respiratory-related influences can also be present during periods of slow respiration (>8.5 bpm).
- The HF band, also known as the respiratory band is the frequency band between 0.15 and 0.40 Hz. This band is connected to the variation in heart rate over the respiratory cycle. During inspiration vagal outflow is inhibited leading to an elevation in heart rate whereas during expiration vagal outflow is increased resulting in a lower heart rate. The HF components are primarily associated with the PNS (Shaffer and Ginsberg, 2017).

Additionally the LF/HF ratio between LF and HF power has become an important indicator thought to represent the balance between the PNS and the SNS, with a low LF/HF ratio representing a high PNS contribution. This however is controversial because the parasympathetic and sympathetic contributions in each frequency band are complex, non-linear and often depend on the resting state and body position of the subject (Kaniusas, 2012)(Choi et al., 2006)(Shaffer and Ginsberg, 2017).

1.1.3 Arterial blood pressure waveform

The blood pressure waveform is divided into 2 parts, the systole and diastole. The systole starts the moment the SL valves open resulting in a large rise of pressure, cumulating in the systolic blood pressure peak P_S. Thereafter the blood pressure decreases until the blood flow reverses and the SL valves close. This results in the dicrotic notch and marks the end of the systole.

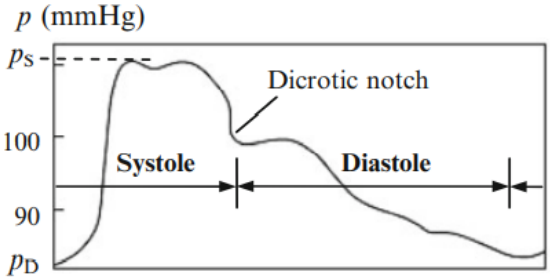

Figure 1·3: An atrial pulsevave during the cardiac cycle. Taken and modified from (Kaniusas, 2012).

The diastole is characterised by a slow decline in pressure until at the lowest point, the diastolic pressure P_D, the SL valves open and the diastole ends. There can be a short rise in pressure at the start of the diastole, due to reflected pressure waves in the arteries (Kaniusas, 2012), as seen in Figure 1·3.

1.2 Baroreflex

The baroreflex mechanism is an essential part in the regulation of blood pressure in humans. Changes in blood pressure, either spontaneous e.g. a change in respiration, or induced through vasoactive drugs, stimulate and activate the Baroreceptors. This induces changes in heart rate, stroke volume and peripheral resistance with the goal to reduce the change in pressure. These changes appear to be dependent on the direction of pressure change, usually exhibiting higher gain and lower setpoint for pressure rise in comparison with pressure fall, resulting in a hysteresis behaviour.

The baroreflex is governed by the autonomic nervous system (ANS), its cardiovagal component is an indicator of the balance between parasympathetic (PNS) and sympathetic (SNS) activities in the modulation of the heart rate.(Kaniusas, 2012) Therefore, the quantitative estimation of the baroreflex has been for decades investigated as an diagnostic tool for the neural regulation at the sinus atrial node. It has been shown that the sensitivity of the cardiovagal baroreflex may provide prognostic value in myocardial infarction (LaRovere et al., 1998), heart failure (Benarroch, 2008) and diabetes (Chapleau, 2012).

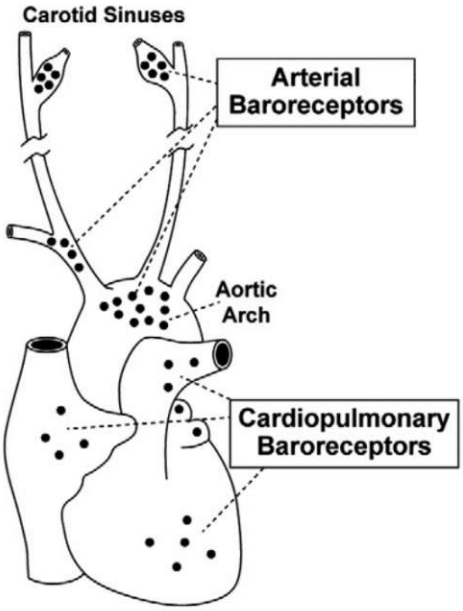

Figure 1·4: Location of the baroreceptors in the cardiovascular system. Taken and modified from (Chapleau, 2012).

The baroreflex functions via a rapid negative feedback loop in which elevated blood pressure stimulates mechanosensitive nerve endings, called baroreceptors, thereby causing the heart rate to decrease. Falling blood pressure reduces baroreceptor activation, causing heart rate to increase and buffering the pressure decrease.

The baroreceptors that govern the baroreflex can be divided into arterial baroreceptors located in major arteries (the carotid sinus and in the aortic arch) and cardiopulmonary baroreceptors that are present in venous blood compartments (primarily, the heart, the vena cava, and the pulmonary vasculature) (Chapleau, 2012), pictured in Figure 1·4.

Over the years several methods have been developed to estimate the *BRS* based on spontaneous fluctuation of blood pressure and heart rate (O'Leary et al., 2003). In older experiments it was common induce blood pressure changes through invasive methods, for example through the administration of of vasoactive drugs, known as modified the Oxford manoeuvrer (LaRovere et al., 1998)(Rudas et al., 1999a). The estimates obtained from these measurements do show correlation with estimates gathered from newer, purely observational experiments. Techniques to analyse the pressure fluctuations commonly used today are the application of linear regression to consecutive sequences of P_S rise with accompanied RR interval increase,

as well as sequences with decreasing P_S and heart RR and spectral power analysis of RR and P_S values in different frequency bands (Laude et al., 2004a). Recently a new method using an elliptical model has been developed to more closely fit the RR-P_S hysteresis pattern (Dabiri et al., 2021).

1.2.1 Arterial baroreflex mechanism

The excitation of baroreceptors rises when blood pressure rises and falls when blood pressure falls. This stimulus is the forwarded into the central nervous system through efferent nerves, where the measured blood pressure is compared to a target reference. The central nervous system then has two mechanism to adjust the blood pressure, neurogenic control by altering the heart rate and stroke volume and myogenic control by altering the peripheral resistance of arteries. The neurogenic control is modulated by both the PNS and the SNS, the myogenic response only by SNS. Any control response of the central nervous system alters the blood pressure, thereby changing the baroreceptor response and forming a feedback loop that can be seen in Figure 1·5.

A sudden blood pressure rise leads to an activation of baroreceptors and therefore an increase of vagal output at the SA, complemented by a decrease in SNS activity. This results in a decrease of heart rate, stroke volume and peripheral resistance leading to a decrease in pressure. The reverse is true for a fall in blood pressure, leading to an increase in SNS, decreased vagal activity, heart rate, stroke volume and peripheral resistance (Kaniusas, 2012).

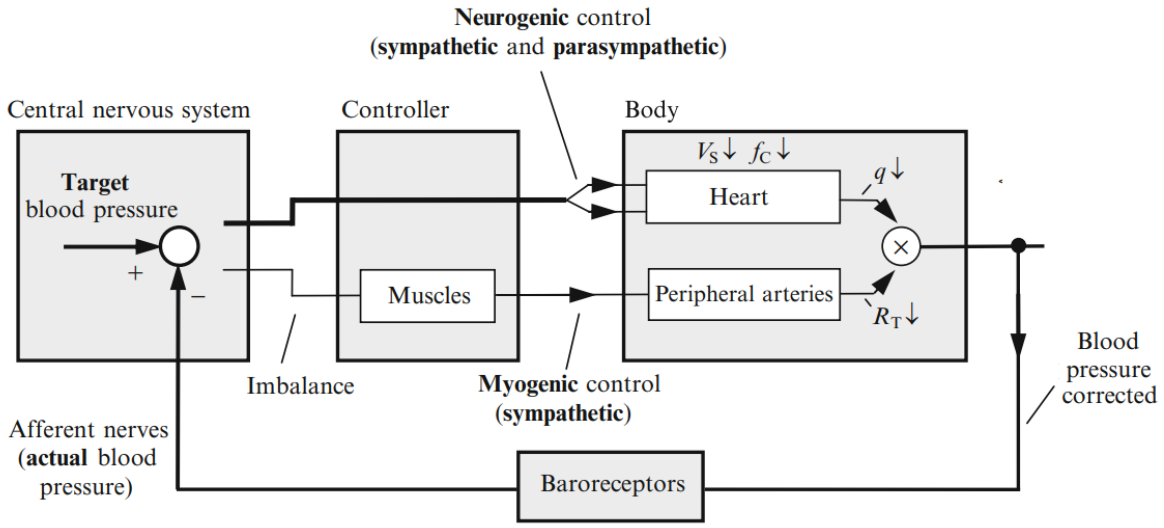

Figure 1·5: A schematic of the baroreflex feedback loop. Taken and modified from (Kaniusas, 2012).

Measurements have found a characteristic cardio vagal baroreflex curve consisting of three zones: threshold, linear and saturation in the pressure range, which was suggested to be fitted to a logistic sigmoid curve, as shown in Figure 6. Measurements are usually conducted with pressures in the linear part of the sigmoid curve (Rea and Eckberg, 1987)(Eckberg and Sleight, 1992).

Abnormalities in the baroreflex function have been linked to neurological diseases that affect the control pathways or to cardiovascular ailments that damage the heart structures. Some examples include damage to the vagus nerve due to diabetes (Chapleau, 2012) or denervation of nerves in heart transplant patients (Raczak et al., 2004). This can result in orthostatic hypotension, the inability to compensate for a pressure drop caused by standing up.

1.2.2 Cardiovagal baroreflex sensitivity

The Cardiovagal baroreflex sensitivity correspond to the vagally mediated baroreflex response, comparing the change of vagal outflow to the change in blood pressure. The level of vagal outflow is directly related to the RR via SA modulation, therefore the *BRS* is typically estimated from the RR-P_S curve. Due to the Baroreflex response being dependent not only on the pressure change itself, but also the rate and direction of the change,with faster and rising pressures having a faster response, a hysteresis behaviour for the *BRS* emerges (Rudas et al., 1999b).

Pressure changes recorded during an experiment can be caused by either spontaneous of external induced changes. Inducing methods include administration of vasoactive drugs(Ler et al., 2010), physical exercise (Incognito et al. 2019), neck suction (Rea and Eckberg, 1987), cold processor test (Hughson et al., 1993). The use of vasoactive drugs to generate a baroreflex response is known as the modified Oxford method (LaRovere et al., 1998). Today *BRS* estimates are mostly generated from the analysis of spontaneous changes.

Hysteresis behaviour

Hysteresis in the cardiovagal baroreflex means that there is a change in the vertical position of the sigmoidal curve (setpoint) and in the linear portion gain (BRS) between ascending and descending sequences (Studinger et al. 2007). For rising blood pressure higher *BRS* and lower setpoint have been estimated, the reverse was observed for falling blood pressure (Kaniusas, 2012)(Studinger et al., 2007) (Dabiri et al., 2021).

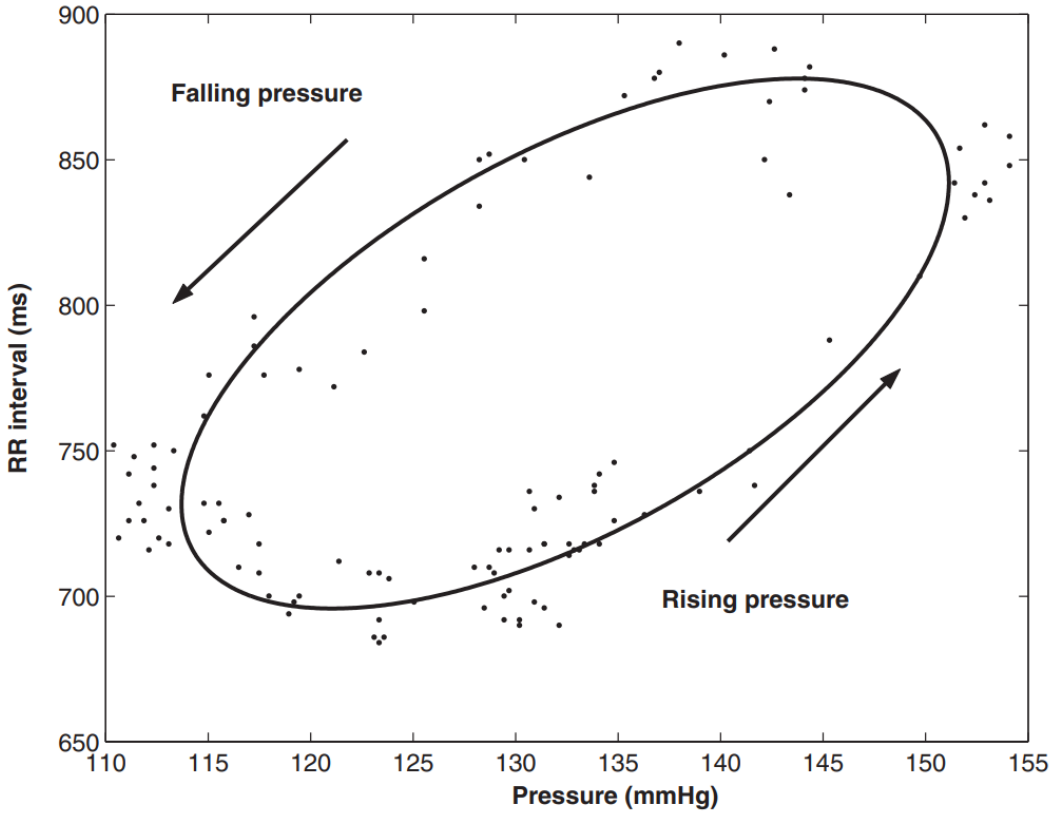

Figure 1·6: Elliptical relation between systolic pressure and RR interval. The arrows indicate the direction of the hysteresis. Taken and modified from (Ler et al., 2010).

Several hypotheses have been put forth to explain this behaviour. Some have suggested that the compliance of blood vessels containing the baroreceptors might behave non-linear, leading to a non-linear baroreceptor response. Others have suggest the non-linearity being of neural origin, for example that there are unmyelinated afferent baroreceptor fibres that begin to fire only at higher pressures (O'Leary et al., 2003) or that there is a central resetting of the baroreflex at the end of the increasing sequence (Ler et al., 2010).

The hysteresis can be geometrically modelled by an elliptical pattern (Eckberg and Sleight, 1992) that encompasses the two sigmoidal RR-P_S curves for rising and falling pressure. A model of the combined ellipse pattern can be seen in Figure 1·6.

Respiration

The respiratory cycle is the primary cause for fluctuation in blood pressure levels and therefore baroreceptor activation. During inspiration, the respiratory muscles contract and the diaphragm lowers, decreasing intrathoracic pressure, forcing air into the lungs. This also causes venous return to the heart to be enhanced, leading to an increase in right ventricular volume of blood. This causes a deviation in the interventricular septum and a decrease in space in the left heart. As a result stroke volume decreases during inspiration, leading to a decrease in P_S.

At the same vagal activity declines, leading to an increase in SA activity and therefore an increase in heart rate. The modulation in SA rate is known as respiratory sinus arrhythmia. During expiration the reverse occurs, with an increase in vagal activity leading to a lower heart rate an higher blood pressure due to higher intrathoracic pressure (Kaniusas, 2012).

It has been observed that the respiratory sinus arrhythmia reaches it maximum at a paced breathing frequency of about 0.1 Hz. This proves useful when observing effects interrelated with the heart rate, such as the baroreflex (Pagaduan et al., 2019). A comparison between spontaneous and paced breathing can be seen in Figure 1·7.

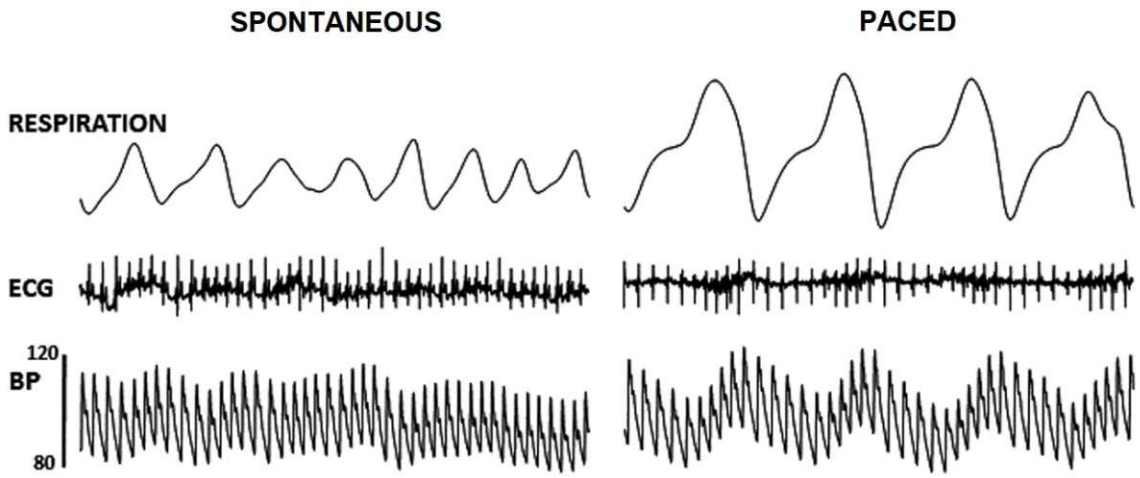

Figure 1·7: Respiration, ECG and blood pressure response to spontaneous and paced breathing. Note the greater variance in P_S, P_D and HRV for paced breathing. Taken and modified from (Pagaduan et al., 2019).

Postural changes

A sudden change in body position from supine to upright, can lead to a drop or increase in venous blood pressure due to gravity action. This can lead to a change in stroke volume as the blood flow and pressure changes, resulting in an activation of the baroreflex and inhibition of the vagus nerve(Lowry et al., 2016). The result is a less pronounced sinus arrhythmia in the upright position(Choi et al., 2006).

Several experiments have observed a change in Cardiovagal BRS between different head up tilt positions. It has been observed that there is a decrease in cardiovagal BRS between supine and 60-degree head up tilt, supine and standing positions using different estimation methods(Choi et al., 2006)(Dabiri et al., 2021)(Taylor et al., 2013).

1.2.3 Sympathetic baroreflex sensitivity

Sympathetic baroreflex sensitivity (symBRS) can be defined as the maximum sensitivity of muscle sympathetic nerve activity to changes in arterial blood pressure.(Short-term sympathetic baroreflex sensitivity increases at lower blood pressures). Muscle sympathetic nerve activity is usually measured via microneurography, whereby a tungsten needle is inserted through the skin into a nerve. Anaesthetics are not required because the procedure induces only minimal discomfort (van Schelvena et al., 2008)(O'Leary et al., 2003)(Hart et al., 2011).

Similarly to the cardiovagal baroreflex, hysteresis effects have been observed in the sympathetic baroreflex, with variations related to age, gender and general health (Hart et al., 2011)(Incognito et al., 2020). For postural changes sympathetic BRS has been observed to show an increase from supine to 60° head up tilt , the opposite trend of the cardiovagal BRS (O'Leary et al., 2003).

1.3 Vagus Nerve

The vagus nerve, also known as the 10th cranial nerve, is a primarily sensory nerve that starts at the brainstem in two bilateral branches and extends through the neck down into the chest and abdomen (Trepel, 2017). The vagus nerve establishes a connection between the brain and major internal organs such as the heart, lungs and the gastrointestinal tract, as well as the circulatory system through the aorta and trachea (Berthoud and Neuhuber, 2000). The activity of the vagus nerve is associated with well being, health and relaxation and adversely related to risk factors like, morbidity, mortality and stress (Thayer et al., 2009)(Zulfiqar et al., 2010).

1.3.1 Vagus Nerve Function

The main function of the vagus nerve is the relay of feedback information from the body's various biosensors to the brain. This includes baroreceptors, mechanical stretch receptors embedded in blood vessels that help to regulate blood pressure, chemoreceptors in the stomach that signal hunger response and thermoreceptors in the liver that help maintain homeostasis (Berthoud and Neuhuber, 2000)(Williams et al., 2016).

Activation of the vagus nerve increases PNS activity and inhibits the SNS. The autonomic nervous system (ANS) then regulates based on vagus nerve feedback, creating a closed feedback loop, with mainly non-linear characteristics. By interacting with the vagus nerve it is possible to interfere with the feedback loop and create a desired neurogenic, myogenic or endocrine response. One example would be the so called carotid massage. A gentle massage of the carotid artery stimulates the baroreceptors of the carotid arch, signalling increased blood pressure to the brain. This causes a decrease in SNS activity, leading to a decline in peripheral resistance and stroke volume. A the same time PNS activity increases, resulting in a slower heart rate (Clancy et al., 2012)(Schweitzer and Teichholz, 1985).

1.3.2 Auricular Vagus Nerve Stimulation

The auricular branch of the vagus nerve (aVN) surfaces as an afferent nerve near the external ear. This allows external stimuli, such as electrical stimulation, to easily access the nerve, resulting in direct pathway to the brainstem. The brainstem even has the ability to forward these stimuli to higher order neurons inside the brain, allowing aVNS to potentially become an affordable non-invasive technique to influence the both the ANS and central nervous system. Since the ANS is made of sympathetic and parasympathetic nerves that modulate the cardiovascular, respiratory, and immunological systems, aVNS can be expected to have systemic effects on the body (Mercante et al., 2018)(Kaniusas et al., 2019a).

So far aVNS has been studied as a treatment for a number of conditions, both in rat models and actual human clinical studies. aVNS has been shown to have positive effects on epilepsy, depression, autism and stroke victims among others (Ben-Menachem, 2000)(Sackeim et al., 2005)(Kaniusas et al., 2019a)(S.Bauer et al., 2016)(E.Hein et al., 2012)(Porter et al., 2011).

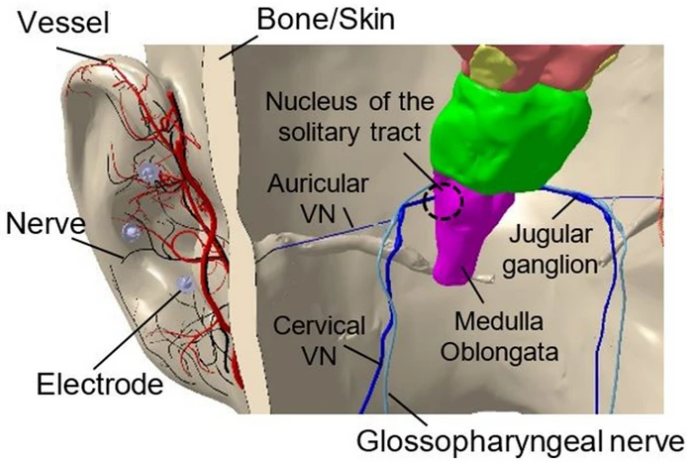

Figure 1·8: Model of the aVN and the placement of electrodes for percutaneous aVNS. Taken and modified from (Dabiri1 et al., 2022).

Transcutaneous aVNS uses non-invasive electrodes placed on the surface of the skin stimulating with a diffuse field whereas percutaneous aVNS is conducted using miniature needle electrodes placed near the aVN or its endings (Bermejo et al., 2017). The latter method can consist of three or four electrodes, with a three phasic stimulation setup producing zero current, eliminating the need for a fourth ground electrode (Dabiri1 et al., 2022). A model for the approximate placement of these electrodes on the outer ear is shown in Figure 1·8. Percutaneous stimulation has the advantage of requiring less energy to stimulate because the signal from the needle electrodes does not have to penetrate the skin barrier and percutaneous aVNS has proven to provide higher efficiency for the applied stimulation patterns (Kaniusas et al., 2020). Compared to the invasive electrodes used in cervical vagus nerve stimulation, the needle electrodes are associated with few side effects, mostly skin irritation due to the wounding (Badran et al., 2018).

1.3.3 Closed Loop aVNS

In traditional aVNS stimulation parameters are obtained beforehand, usually based on the patients vitals as well as a perception test to generate a comfortable, but noticeable tingling feeling well below the pain threshold. While this method can generate a rough estimate based on the stimulation patterns, the underlying physiological processes may well be over- or under-stimulated leading to sub optimal therapeutic outcomes. For example the response of the ANS to aVNS seems to be both frequency and pulse width dependent, with higher frequencies (20–250 Hz) activating the parasympathetic system and low frequencies (0.5–10 Hz) activating both parasympathetic and sympatric nervous systems (Kaniusas et al., 2019a).

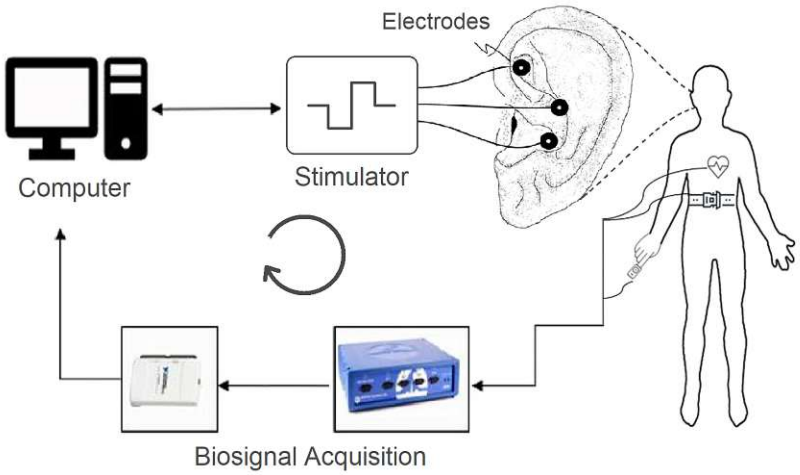

Figure 1·9: A diagram of an experimental closed auricular vagus nerve stimulator setup. Taken and modified from (Kaniusas et al., 2019b).

The human body is a complex and interdependent system, where any stimulus may inadvertently reinforce or alter its physiological state. To account for those changes, especially those induced through the use of aVNS, sensory feedback should be applied to the stimulation parameters to adjust intensity and timing for more effective control. Previous work has shown the ability to control the heart rate in sheep or pigs using closed loop VNS(Badran et al., 2018) as well as reducing seizure frequency in epileptic patients (Cook et al., 2020). These studies however all used invasive cervical vagus nerve stimulators. Non-invasive closed loop aVNS systems are just now being developed with a recent study investigating the effect of transcutaneous vagus nerve stimulation triggered by muscle activation for neurorehabilitation.

Today several experimental stimulators are being designed with signal acquisition and processing features for ECG, PPG and respiration signals. These biosignals can then be used as biofeedback for aVNS sessions, for example to alleviate symptoms in patients with peripheral blood perfusion, cardiac or baroreflex disorders (Napadow et al., 2012)(Dabiri1 et al., 2022). A schematic of a closed loop aVN stimulator is shown in Figure 1·9.

1.4 Measuring Devices

Here a short overview of the available recording devices is presented.

1.4.1 Caretaker-Medical Vitalstream™ Sensor

Figure 1·10: A photo of the Vitalstream™ finger cuff sensor(right) and the VIVALNK Bluetooth ECG monitor(left)

The Caretaker-Medical Vitalstream™ finger cuff sensor is is a non-invasive medical device used to measure haemodynamic parameters such as blood pressure and arterial tone changes. It relies on a technique called pulse e decomposition analysis, where it is assumed that two central reflection sites of the arterial pulsewave, one at the aortic junction between thorax and abdomen, the other at the iliac arteries in the pelvis, are responsible for the shape of the blood pressure pulsewave in the upper body. The reflection coefficients of those sites are highly depended on the blood pressure and thereby offer a tool to calculate blood pressure parameters. Based on the timing of the reflected peaks in relation to the systolic peak a proprietary algorithm was developed to accurately calculate P_S, P_D and mean arterial blood pressure at each heartbeat. Once a sensor has been calibrated the algorithm can even adjust to changes in body position with any recalibration (Baruch et al., 2011).

The sensor itself is wireless and can be combined with other wireless sensors to offer more monitoring options. One of them, the VIVALNK ECG patch is a wireless Bluetooth heart monitor that records the ECG signal synchronised to the Vitalstream™ device at 128 Hz. SPO2 and temperature sensors are also devices that are currently availiable (Caretaker, 2021). The Vitalstream™ and VIVALNK sensors can be seen in Figure 1·10.

1.4.2 Portapres®

Figure 1·11: A photo of the Portapres® blood pressure measuring device

The Portapres® sensor is an instrument to continuously measure the arterial blood pressure waveform in the fingers. Its function is based on the volume-clamp method and it can be operated as a portable device using large batteries. The device can be set to output P_S, P_D or the whole pressure waveform as an analog signal (Eckert and Horstkotte, 2001).

1.4.3 BIOPAC MP36 System

Figure 1·12: A photo of the BIOPAC System with ECG electrodes (left) and a respiration belt sensor (right)

The BIOPAC MP36 is a 24 bit A/D converter system used as part of the recording chain for the biosignals. A software suite called BSL Pro is used to control the Biopac system and set up various measuring parameters, such as sampling rates, gain and input filters. The

BIOPAC system offers a number of recording peripherals, of witch the ECG and respiration belt were used. The Portapres® system also connects to the BIOPAC (BIOPAC Systems Inc.,).

1.4.4 Closed Loop aVN Stimulator

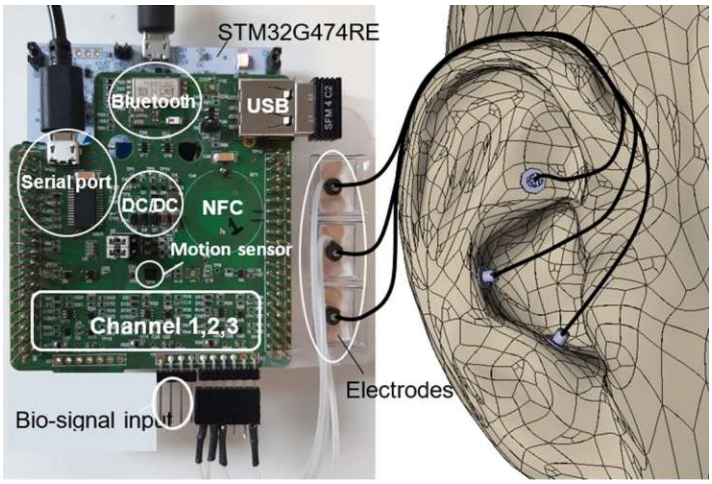

Figure 1·13: The prototype closed loop aVN stimulator used in this work. Developed by (Dabiri1 et al., 2022).

The experimental closed loop aVN stimulator used in this work was recently created by members of this institute (Dabiri1 et al., 2022). The stimulator is capable of delivering mono-phasic, bi-phasic, or tri-phasic stimulation with variable intensity and pulse width. Stimulation amplitude is currently set between 0V and 1.8V, with the current limited to below 1 mA. For closed loop application, the stimulator is capable of receiving inputs of pulse plethysmography (PPG), ECG and respiration belt signals, it is however limited to only one input at a time. For the duration of this work all input signals were recorded on the BIOPAC system and then forwarded to the stimulator in real time, to account for any errors in the experimental device. The system is controlled through MATLAB software running on a PC. A graphic showing the stimulator can be seen in Figure 1·13.

Chapter 2

Methods

In this chapter the experimental setups and the methods used to obtain the results are presented are presented. Two different sets of experiments were preformed, the first conducted an investigation into the effects of Head-Up-Tilt postural changes on the baroreflex, the second investigated the effects of synchronised vagus nerve stimulation on the cardiovascular system.

2.1 Head-Up-Tilt Measurement

In this section the Head-Up-Tilt experiment is described. This experiment aims to provide *BRS* estimations using both linear regression and the novel ellipse method for a set of different Head up tilt positions. Seven subjects, their physiological data shown in Table 2.1, voluntarily agreed to participate in the investigation. All participants were informed beforehand about the precise course of the experiments and signed a waiver acknowledging laboratory safety instructions. The measurements were conducted non-invasively, with at least one other person present throughout. All recorded data and personal information was anonymized in accordance with valid data protection guidelines.

	Age	Weight	Height	BMI
Subject 1 (M)	32 Y	183 cm	86 kg	25.7 kg/m^2
Subject 2 (M)	23 Y	180 cm	65 kg	20.1 kg/m^2
Subject 3 (F)	31 Y	168 cm	56 kg	19.8 kg/m^2
Subject 4 (M)	34 Y	173 cm	67 kg	22.4 kg/m^2
Subject 5 (M)	25 Y	186 cm	65 kg	18.8 kg/m^2
Subject 6 (M)	24 Y	177 cm	78 kg	24.9 kg/m^2
Subject 7 (F)	26 Y	163 cm	52 kg	19.6 kg/m^2

Table 2.1: The data of the 7 subjects that participated in the Head-Up-Tilt experiments.

2.1.1 Experimental Protocol

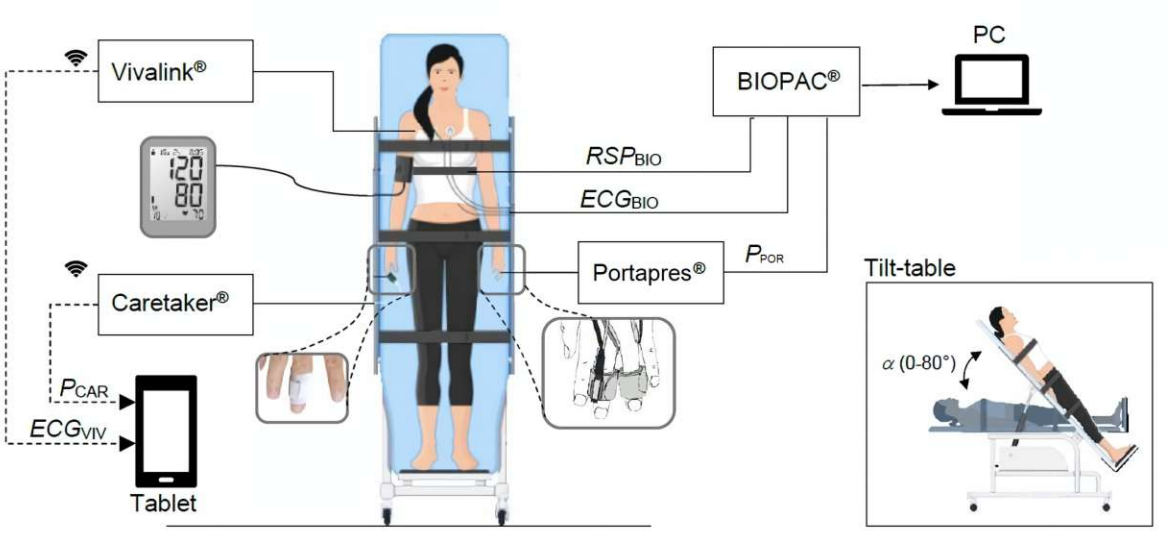

Figure 2·1: A schematic of the experimental setup. The subject is placed on a tilting bed and connected to the BIOPAC sensors (right) and the Vitalstream™ device (left).

Each subject was placed on a tilting bed, capable of tilting between 0 degree(bed is horizontal) and 80 degree angles, in the supine position. The subject was then fitted with a respiration belt, ECG electrodes connected at both wrists and the right leg and the Portapres® blood pressure recording device on the left middle finger, all connected to the BIOPAC ADC system. The sampling rate was set to 1000 Hz. Furthermore the Caretaker-Medical Vitalstream™ blood pressure cuff was connected to right middle finger and the VIVALNK Bluetooth ECG sensor was placed on the left side of the chest slightly above the heart. The second ECG was used as a synchronising signal between the BIOPAC and the Vitalstream™ systems.

After ten minutes in supine position, to allow for cardiovascular parameters to settle, the subject was instructed to begin a 10 second paced breathing cycle (5 seconds inspiration, 5 seconds expiration). A paced breathing cycle was chosen to increase and lengthen the baroreflex response. The subjects heart rate and blood pressure were then recorded for a period of 10 to 11 minutes. Afterwards the subject was instructed to breathe normally again and the angle of the tilting bed was changed to 30 degrees head up tilt. After a 3 minute rest to again settle cardiovascular parameters the measurement resumed with the same 10 second paced breathing cycle for another 10 to 11 minutes. This same procedure was again performed for a 60 degree and then an 80 degree head up tilt position. For the last measurement the subject

was asked to step off the tilting bed and following a 3 minute pause, followed the same 10 second paced breathing protocol in a standing position. Afterwards, while the subject was still standing three reference blood pressure measurements were taken with a blood pressure cuff, to ensure the readings of the measuring devices were accurate.

2.1.2 Signal Processing

During preparatory measurements the Portapres® Blood pressure cuff was proven unreliable for a change in body positions. Because the MAP offset is provided via 2 sensors, any inaccuracy during placement or any misalignment during the measurements leads to false pressure readings. The Vitalstream™ blood pressure cuff was therefore chosen to provide the MAP reference, the 2 sensors were synchronised through the ECG signals recorded by the BIOPAC and Vitalstream™ respectively. The mean distance between P_S and P_D of both recordings was calculated and the Portapres recording was offset to match the Vitalstream™ reference.

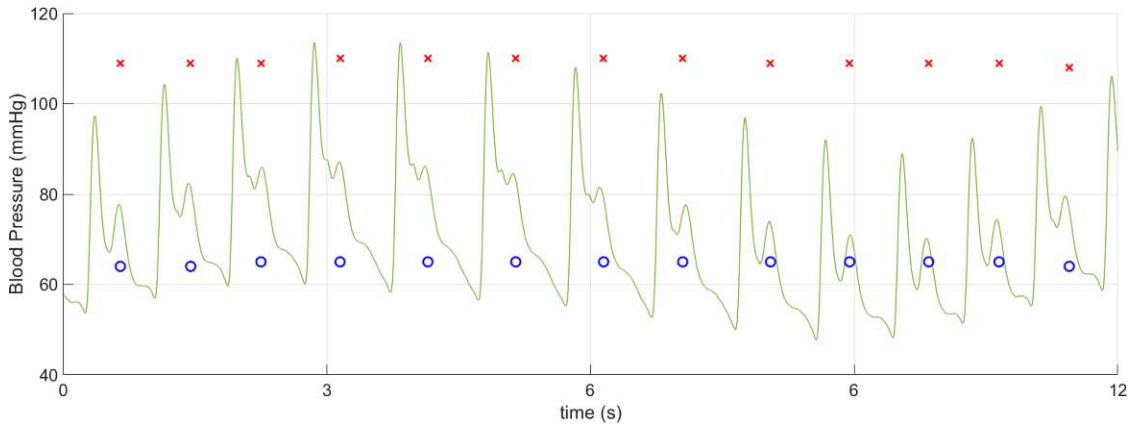

Figure 2·2: The continuous Portapres® signal(■) overlayed with the calculated P_S(■) and P_D(■) values of the Vitalstream™ device.

The RR, P_S and P_D values for the recordings, used in the analysis in section. were extracted using the findpeaks function in MATLAB R2021b (The MathWorks Inc.). Some of the subject's ECG recording had to be adjusted, their R peaks too small for the algorithm to recognise. Here the R peaks were found using the prominent S-peaks as reference and then amplified. Each adjustment was manually verified.

2.1.3 Ellipse Method

This method follows the methodology pioneered by (Dabiri et al., 2021). The extracted RR and P_S were searched for sequences of at least 3 consecutive ascending or descending RR and corresponding P_S values. To primarily represent the cardiovagal BRS, only sequences that had at least an 85 percent mutual correlation coefficient were accepted, with no minimum difference thresholds for the sequence to be considered valid. A spontaneous cardiovagal baroreflex cycle (CBC) was formed when an up or down sequences was immediately followed by an opposite sequence, completing the up and down cycle. Each sequence could be part of 2 different CBCs, a CBC joined with the preceding sequence or a CBC with the following sequence. Therefore, n consecutive up and down sequences (with n > 2), can result in a maximum of (n-1) CBCs. An example CBC identified by this method is shown in Figure 2·3

Ellipses approximating the CBC are created as follows. First all the points of the CBC are drawn onto a 2D plane, with P_S and RR as the x and y axis, and a polygon is drawn connecting all points in order. Then an ellipse is created, fitted so it encompasses all the CBC points while containing the minimum area. This was via the Khachiyan algorithm, an iterative method for minimizing convex functions (Kumar and Yildirim, 2005). The ellipses were then downscaled to exhibit the same area as the polygon, the center and orientation were kept the same, as shown in Figure 2·4.

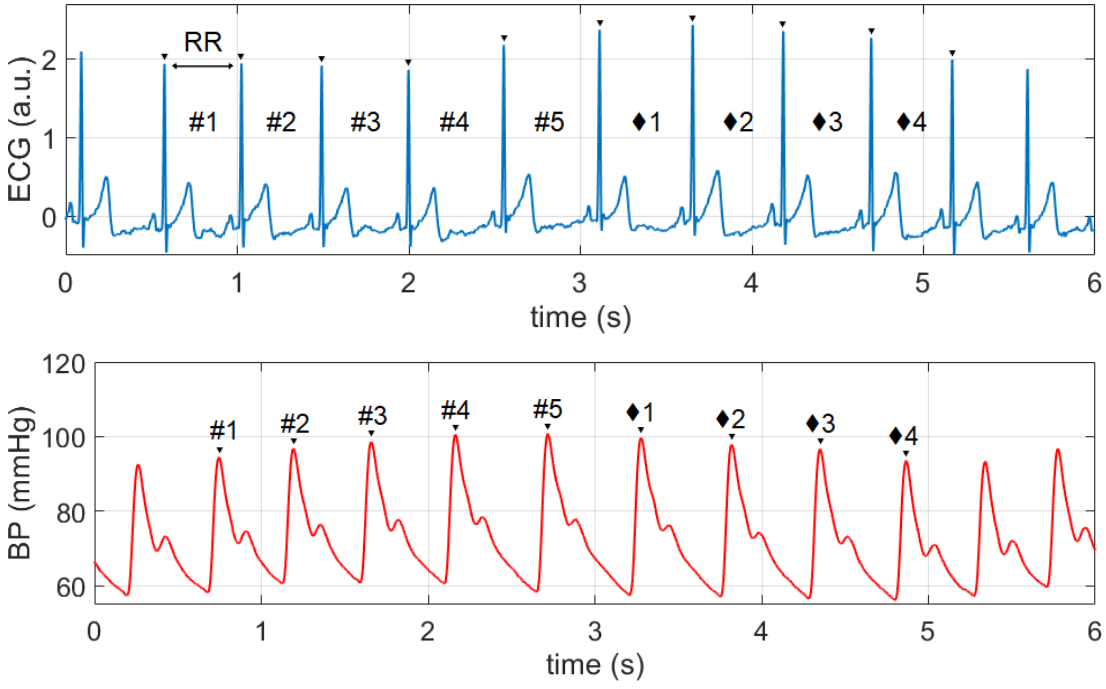

Figure 2·3: Example P_S (■) and RR(■) values of a CBC sequence identified by the ellipse method. Data from subject 2 in supine position.

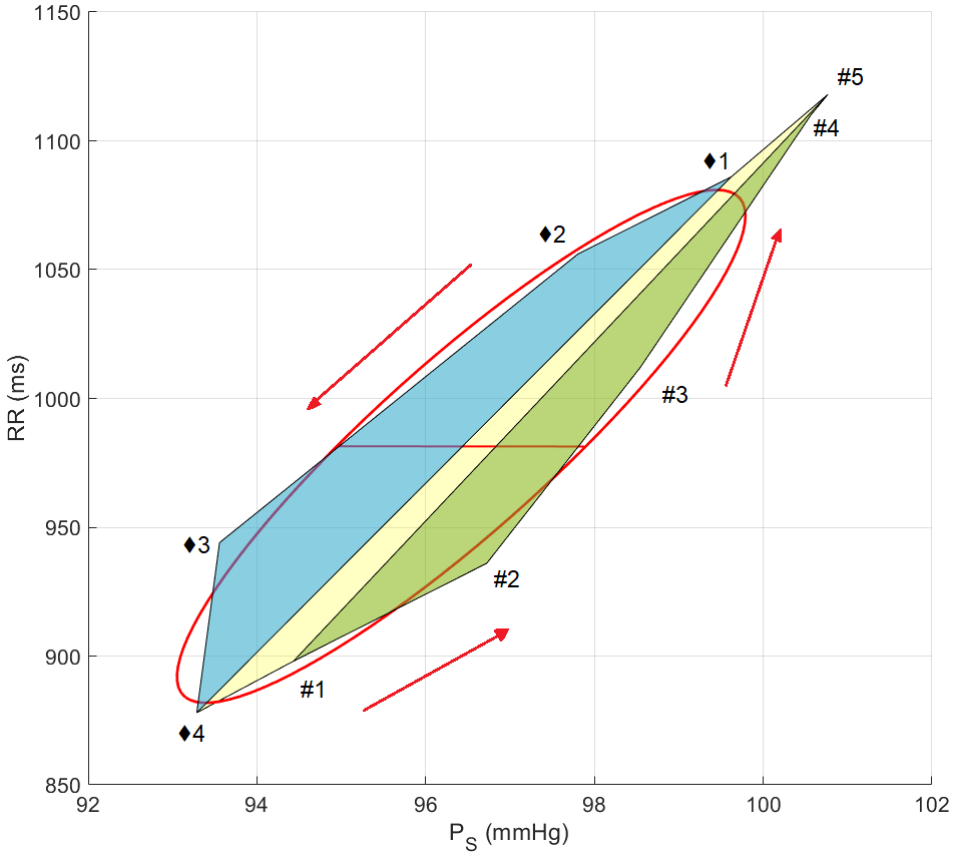

Figure 2·4: An example of the ellipse method. The up sequence (■) and down sequence(■) areas are combined at the end, the ellipse is then fitted to the sequence point and scaled to match the shaded area. Data from subject 2 in supine position.

Ellipses approximating the CBC are created as follows. First all the points of the CBC are drawn onto a 2D plane, with P_S and RR as the x and y axis, and a polygon is drawn connecting all points in order. Then an ellipse is created, fitted so it encompasses all the CBC points while containing the minimum area. This was via the Khachiyan algorithm, an iterative method for minimizing convex functions (Kumar and Yildirim, 2005). The ellipses were then downscaled to exhibit the same area as the polygon, the center and orientation were kept the same, as shown in Figure 2·4

In the case the the up and down sequences of the CBC were overlapping a slightly different technique was used. Here the shape drawn 2D shape of the connected CBC points is not one polygon, but multiple depending on the number of sequence overlaps. For each of these smaller polygons an individual sub-ellipse is created using the method above. From

these sub-ellipses the ellipse was constructed using weighted parameters for both center coordinates and the orientation angle. The area A is calculated as the sum of all sub-ellipse areas. Because the orientation angles are in the range of ±1 % the major axis length a was calculated as the sum of the sub-ellipses major axes. The minor axis b is also calculated from weighted sub-ellipse parameters.

The parameters for all CBSs are represented by the created ellipse's center coordinates, axis lengths and orientation angle. The value of BRS for CBC is estimated out of θ_0 based on $BRS = \tan^{-1} \theta_0$.

2.1.4 Linear Regression

A linear regression was performed on up-, down- and completed CBC sequences, using individual RR and P_S parameters. This provided another estimate for the BRS.

2.2 Vagus Nerve Stimulation

In this section the synchronised aVNS experiment is described. Five subjects volunteered to participate, their physiological data is shown in Table 2.2. All participants were informed beforehand about the scedule of the experiments and signed a waiver acknowledging laboratory safety instructions. The measurements were minimally-invasive, a trained medical professional administered the placement of the percutaneous aVNS electrodes and was present throughout. All recorded data and personal information was anonymized in accordance with valid data protection guidelines.

	Age	Weight	Height	BMI
Subject 1 (M)	32 Y	183 cm	83 kg	24.8 kg/m^2
Subject 2 (F)	31 Y	168 cm	56 kg	19.8 kg/m^2
Subject 3 (F)	20 Y	160 cm	58 kg	21 kg/m^2
Subject 4 (M)	22 Y	177 cm	56 kg	17.9 kg/m^2
Subject 5 (M)	49 Y	178 cm	80 kg	25.2 kg/m^2

Table 2.2: The data of the 5 subjects that participated in the aVNS experiments.

2.2.1 Stimulation Protocols

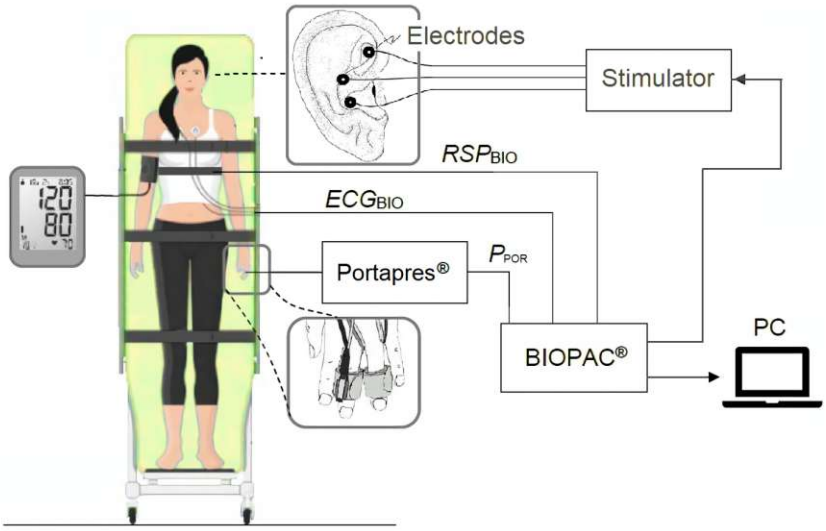

Figure 2·5: A schematic of the closed loop aVNS experiment.

2 different experimental protocols were created to investigate different aspects of closed loop tri-phasic aVNS application. All protocols consisted of a setup procedure, whereby the aVNs electrodes were placed and the subjects stimulation perception, and pain threshold were discovered. Each subject had the 3 electrodes placed on the left ear, their positions can be seen in Figure 2·6. Blood pressure, ECG Respiration and the stimulation impulse were recorded with the BIOPAC and Portapres® sensors at a sampling frequency of 1000 Hz. The subjects were in a seating position with normal respiration, each subject preformed each protocol twice for a total of 5x2x2 = 20 measurements. A schematic showing the stimulation experiment can be seen in Figure 2·5.

Figure 2·6: Stimulator electrode placement on the left ear, subjects 1-5.

Cardiac-gated aVNS

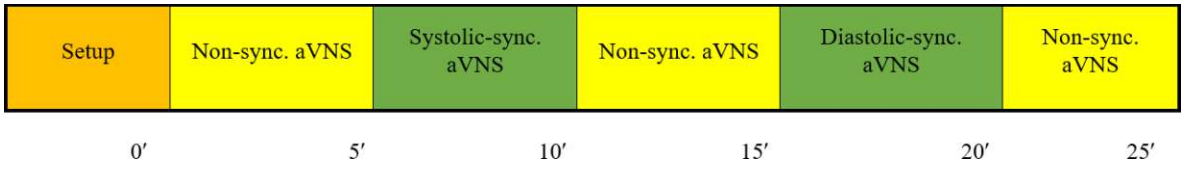

Figure 2·7: The Protocol for Cardiac-gated aVNS

This experiment was preformed to investigate the effectiveness of aVNS synchronised to the different phases of the cardiac cycle. The experiment was conducted in 5 5-minute segments (pictured in Figure 2·7), three segments of non-synchronised aVNS with a 1-second interval between stimuli, and one segment each for stimulation synchronised to the systole and diastole respectively. The stimulation was conducted using triphasic pulses with an individual width of 3ms and a combined stimulation pulse width of 300ms. The stimulation intensity was dialled in to each subjects comfort level beforehand.

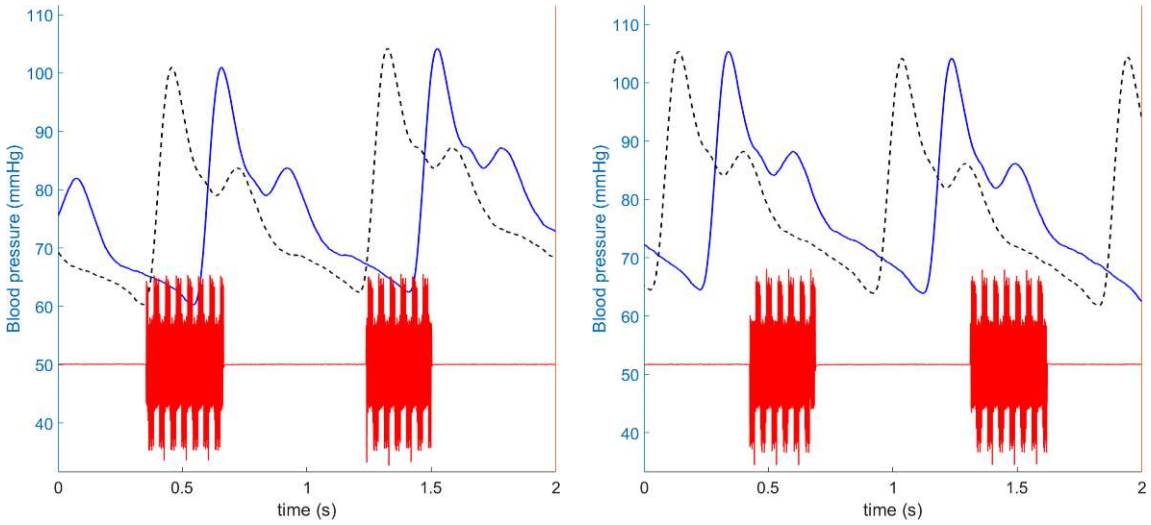

(a) Systolic sync. aVNS **(b)** Diastolic sync. aVNS

Figure 2·8: The cardiac gated stimulation signal(■) overlaid with the blood pressure(■). The pressure signal is taken at the finger, therefore a delay of -0.2s for systolic and 0.2s for diastolic synchronisation is added. The striped signal shows the -0.2s delayed pressure signal(■) at the approximate time it leaves the heart.

To synchronise the stimulation to the systole or diastole a delay of ±0.2s is added to the expected arrival of the systolic peak at the blood pressure finger cuff sensor. This ensures that the blood pressure wave, travelling with a pulse wave velocity of about 5 m/s and a heart to finger distance of about 1m, reaches the sensor in approximately 0.2s (Kaniusas, 2012). The stimulation therefore occurs when the heart is at the systolic peak or 0.4s after the systolic peak, in the midst of the diastole. An example of this can be seen in Figure 2·8

Respiratory-gated aVNS

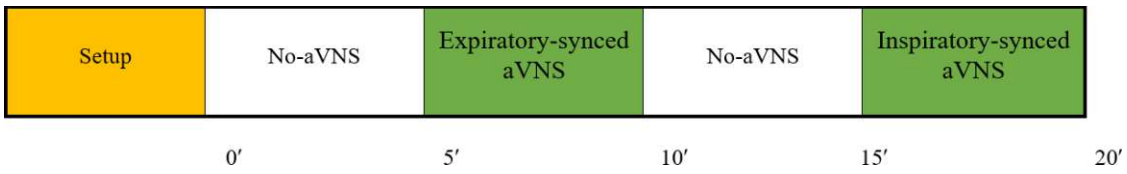

Figure 2·9: The Protocol for Respiratory-gated aVNS

The second protocol investigates the effect of respiratory gated aVNS on the cardiovascular system. Here the experiment was divided into 4 5-minute segments, 2 segments of no stimulation and one segment each of expiration and inspiration synced aVNS. Once again triphasic pulses with an individual width of 3ms were used, the total stimulation time was governed by the respiration signal. The detailed protocol is shown in Figure 2·9

2.2.2 Time and frequency analysis

P_S, P_D, and RR values of the recorded data was extracted using the MATLAB R2021b findpeaks function. The ECG signal of some subjects also had to be adjusted, similar to the methods used in section.

SDNN: The SDNN(Root Mean Sum of Squared Distance)(Shaffer and Ginsberg, 2017) is a measure for the activation of the Autonomic nervous system, it is modulated by both the PNS and SNS. It is correlated with the ULF, VLF and LF band power. Because the SDNN value increases with the total measuring time, only measurements of equal length should be compared using this value. The SDNN is calculated using the following formula:

$$SDNN = \sqrt{\frac{1}{N-1}\sum_{i=1}^{N}(RR_i - \overline{RR})^2} \tag{2.1}$$

The RMSSD(Root Mean Square of Successive Differences)(Choi et al., 2006) reflects the timing variability between successive Heartbeats, it is used as an estimation for vagally mediated changes in the HRV. It is correlated with HF power and exhibits a stronger relation to the PNS than the SDNN. It is calculated the following way:

$$RMSSD = \sqrt{\frac{1}{N-1}\sum_{i=1}^{N-1}(RR_{i+1} - RR_i)^2} \tag{2.2}$$

Frequency domain

The *RR*-Values for each 5 minutes segment were resampled at 4 Hz by linear interpolation to construct equidistantly spaced time series. The mean value was then subtracted from the signal to remove the DC content, corresponding to non-harmonic components in the VLF region.

A Fourier transformation was preformed and the power spectral density of the signal was calculated. For the analysis of the power spectral density two frequency bands of interest, the LF and HF bands, were isolated.

Chapter 3

Results

In this chapter, the results obtained in this work are presented.

3.1 Head-Up-Tilt

This section shows the results of the Head-up tilt experiment. First the measurement itself is discussed, then the results of the ellipse method *BRS* estimates are presented and lastly the Baroreflex cycles are analysed heartbeat by heartbeat.

3.1.1 Signal Parameters

Blood Pressure

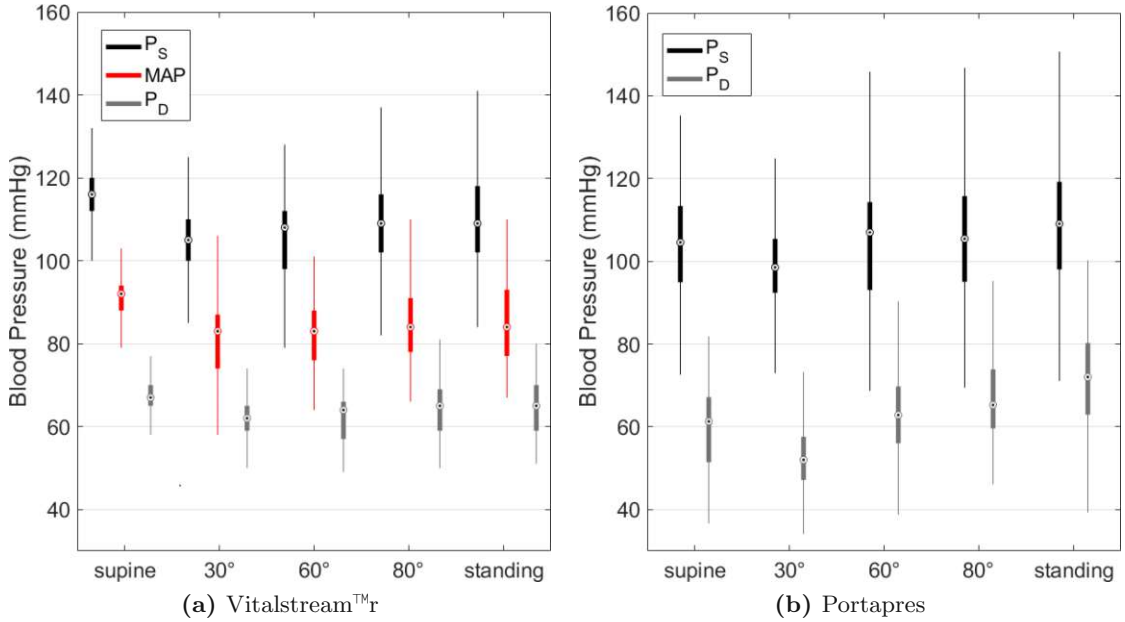

(a) Vitalstream™r **(b)** Portapres

Figure 3·1: P_S(■), MAP(■) and P_D(■) values for the Vitalstream™ sensor and the adjusted Portapres® signal

As discussed in the Methods chapter the blood pressure measurement was adjusted to the values recorded by the Vitalstream™ sensor. Because this device does not measure blood pressure values directly but calculates them per heartbeat, any irregular measurement can result in missed outputs. The sensor also does not adjust well to rapid changes in blood pressure, as were produced through the paced breathing. The Vitalstream™ sensor therefore provided only an estimate for the mean BP level. The measured P_S and P_D values for the Vitalstream™ and the adjusted Portapres® signal can be seen in Figure 3·1. The much slower response to the Baroreflex induced pressure changes can be clearly seen by comparing the width of each distribution. Also clearly noticeable is the difference in blood pressure values for the supine and 30 degree tilt position. This can be explained by the fact that for some of those measurements the Vitalstream™ sensor struggled to calculate blood pressure values, leading to a lower number of data points for some subjects, thereby skewing the distribution.

	Supine	30°	60 °	80 °	Standing
Heart rate (1/min)	70.9 ± 9.4	73.7 ± 9.7	88.7 ± 12.2	94.6 ± 13.6	95.6 ± 13.5
P_S (mmHg)	103.5 ± 13	99 ± 10.8	104.8 ± 14.8	106 ± 15.8	108.9 ± 14

Table 3.1: P_S and heartrate (bpm) for all positions, mean ± std

Respiration

Supine	30°	60 °	80 °	Standing
6 (6.02 ± 0.58)	5.97 (6.01 ± 0.64)	6 (6.03 ± 0.48)	6 (6.03 ± 0.62)	5.98 (6 ± 0.53)

Table 3.2: Paced breathing, respirations per minute, median (mean ± std)

The Respiration frequency for all positions is shown in Table 3.2. It can clearly be seen that for all positions the subjects held the same paced breathing frequency of $f_R = 0.1$ Hz.

3.1.2 Ellipse Method

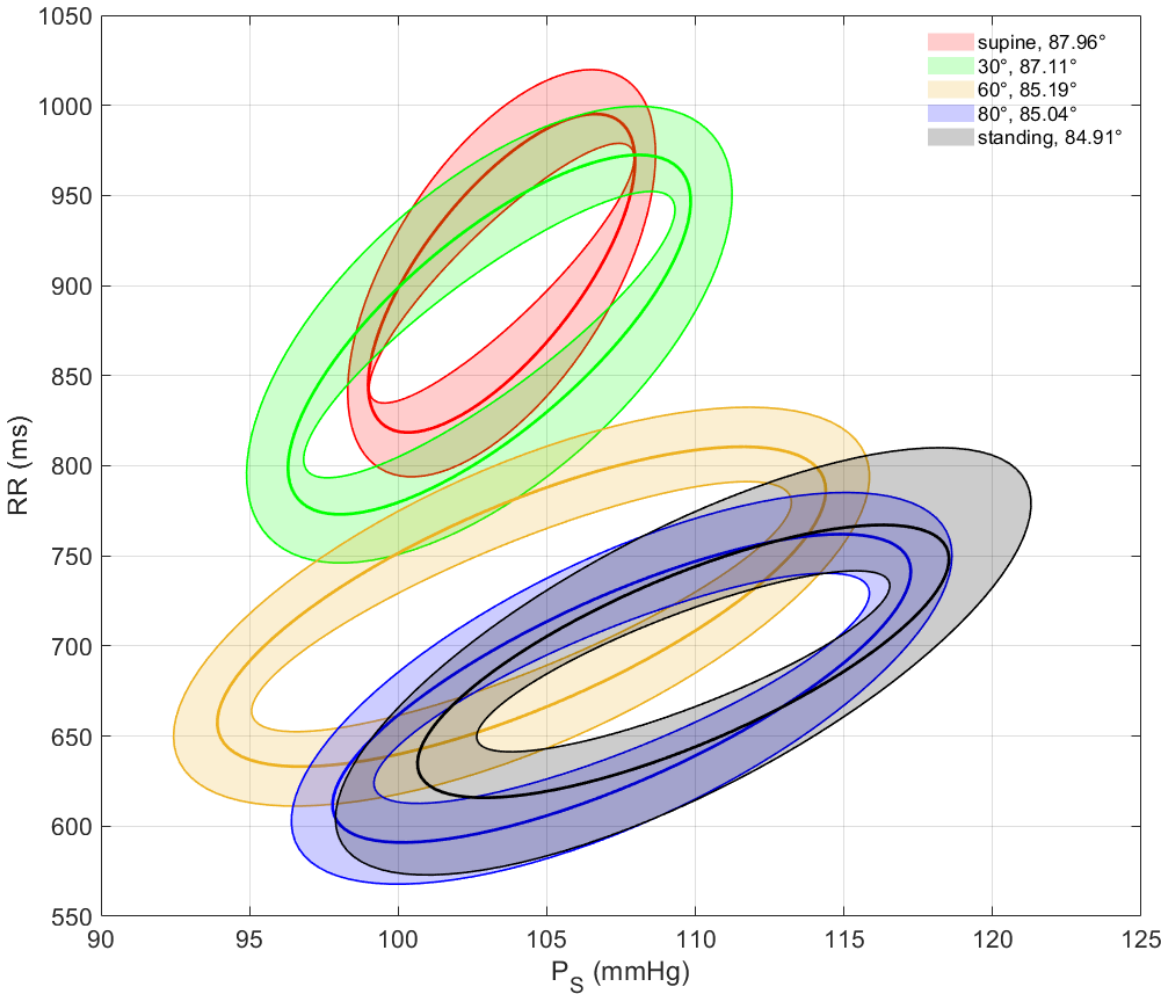

Figure 3·2: The resulting baroreflex ellipses, combined for all subjects, over supine(■), 30° Head-up tilt(■), 60° Head-up tilt(■), 80° Head-up tilt(■) and standing(■) positions. Median ellipse angles are shown in the legend.

The results obtained from the ellipse method presented in Chapter 2 can be seen in Figure 3·2. It shows the estimated hysteresis ellipses for the supine, 30°, 60°, 80° head up tilt and the standing position, with the middle ellipses representing the median value of axis length and orientation angle, the inside and outside ellipses representing the 25th and 75th quartile and the shaded area constituting the interquartile range (IQR). The ellipses are centered around the median centroid value for each position. The parameters for each ellipse are shown in Table 3.3.

	Supine	30°	60 °	80 °	Standing
Orientation angle θ_0					
25th quantile	86.86°	86.07°	83.73°	83.82°	83.37°
Median	87.96°	87.11°	85.19°	85.04°	84.91°
75th quantile	88.46°	87.73°	86.03°	86.01°	85.82°
Major axis length a					
25th quantile	72.2	79.7	69.8	64.3	50.6
Median	88.4	99.9	89.1	85.9	76
25th quantile	113	126.8	111	108.9	118.9
Minor axis length b					
25th quantile	2.07	3.05	4.96	4.68	3.8
Median	3.19	4.53	7.02	6.32	5.89
75th quantile	4.2	6.45	8.86	8.15	7.89

Table 3.3: Median values and IQR of the main ellipse characteristics.

The median value of the major axis a compared to the supine position changes to 113%, 101%, 97% and 86% for the 30°, 60°, 80° and standing positions. The minor axis b median value only increases however, reaching 142%, 228%, 255% and 247% for 30°, 60°, 80° and standing positions. Lastly the median *BRS*, calculated from the orientation angles, decreases to 71%, 42%, 41% and 40% for the 30°, 60°, 80° and standing positions, mirroring the decrease in the median orientation angle.

It should be noted that although the Orientation angles, and therefore the *BRS* estimate are very representative of the overall dataset, there exists significant variation in ellipse size and position between the subjects. Figure 3·3 shows the ellipse estimates for each subject with sufficient CBCs, illustrating the difference between individuals.

Figure 3·4 shows the decomposition of the ellipses from Figure 3·2, with *RR* and P_S values plotted over a normalised respiration cycle of 360°. As before the values are presented as the median and 25th and 75th quartile, with the inner 25th quartile curve having the lowest variance, the outer 75th the highest. The shaded area represents the IQR of the series.
Table 3.4 presents the median phase difference of the *RR* and P_S values, with decreases of 3.5°, 2°, 4.9° and 4.2° between the supine and the 30°, 60°, 80° and standing position . The median *RR* deflection for 30°, 60°, 80° and standing position also changes to 113%, about 100 %, 97 % and 86% compared to the supine position. The median P_S deflection however rises for all positions to 150%, 228%, 217% and 199% of the supine value for the 30°, 60°, 80° and standing position respectively.

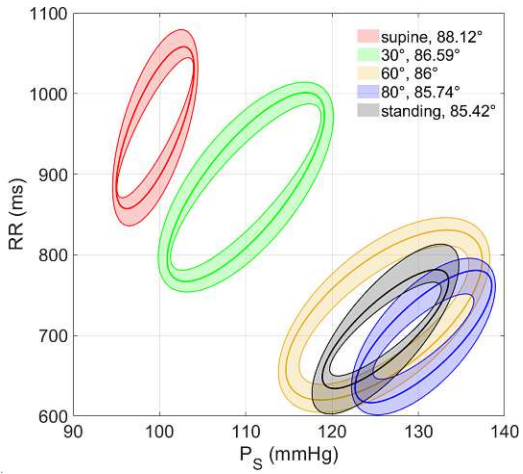

(a) Subject 2

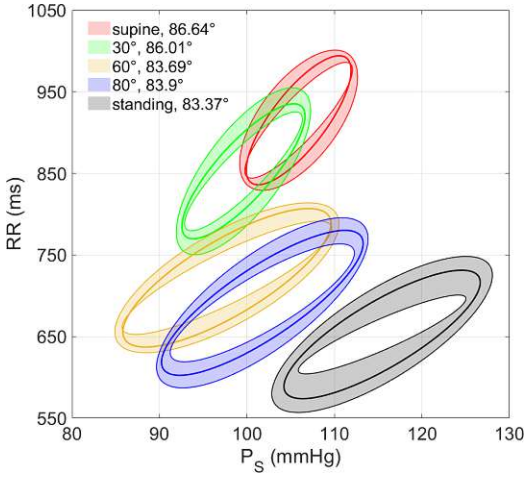

(b) Subject 3

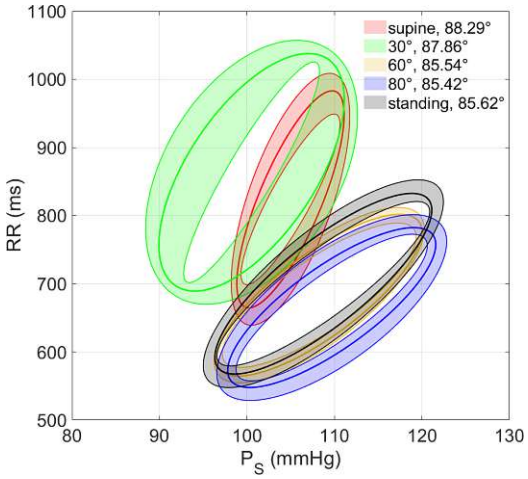

(c) Subject 4

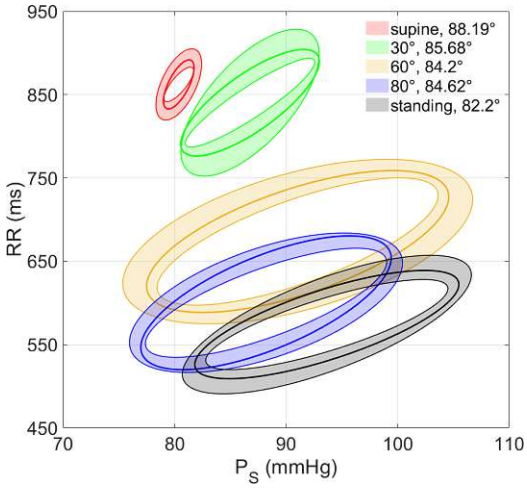

(d) Subject 5

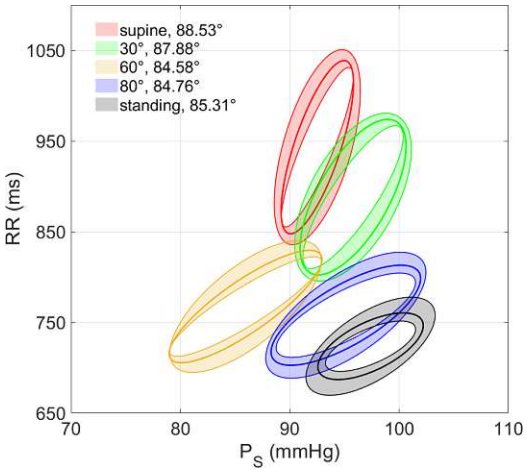

(e) Subject 7

Figure 3·3: Ellipse method for each subject with sufficient data. Median ellipse angles for supine(■), 30° Head-up tilt(■), 60° Head-up tilt(■), 80° Head-up tilt(■) and standing(■) positions are shown in each figure.

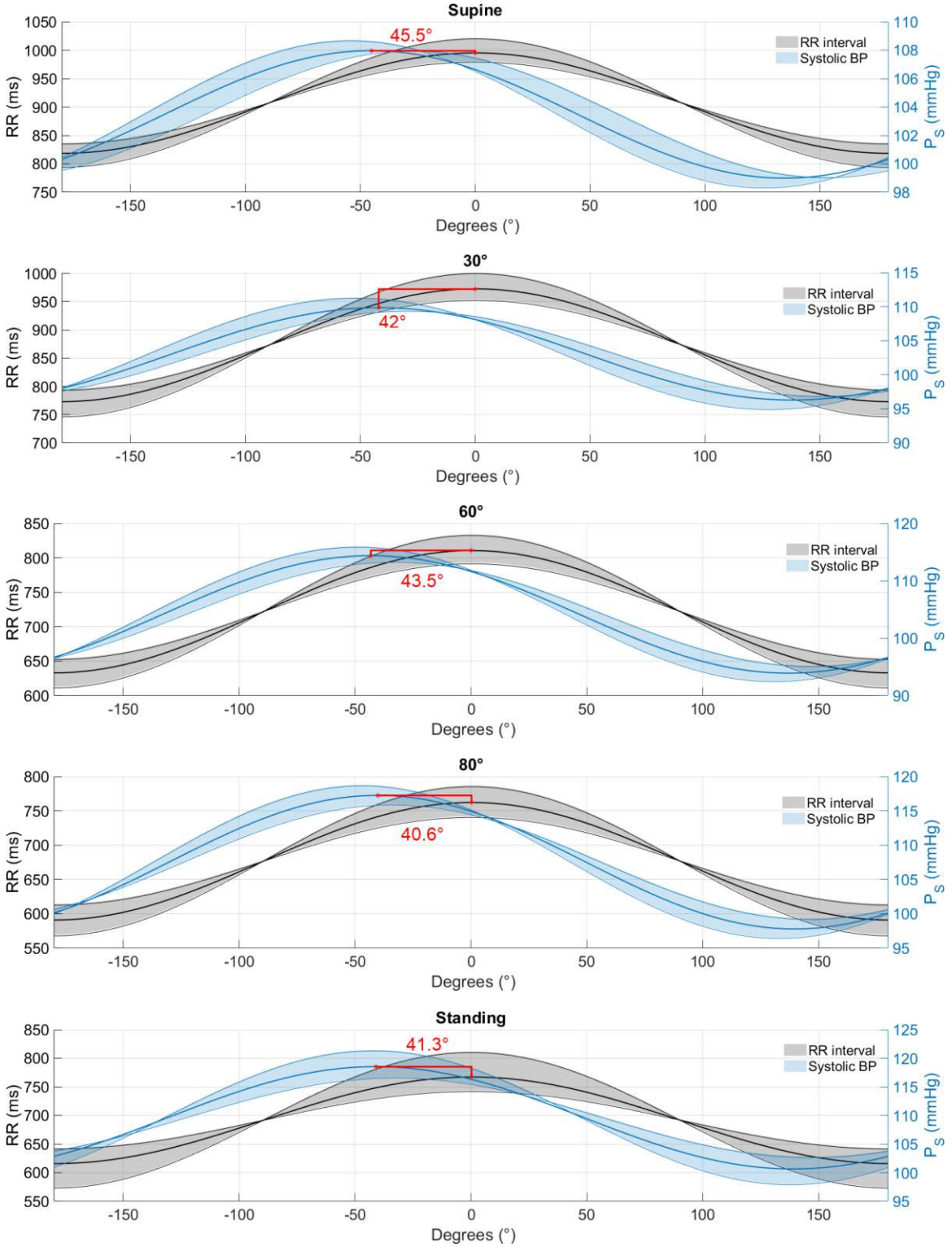

Figure 3·4: P_S(■) and RR(■) courses for the median and IQR ellipses of the spontaneous CBC for all Head-up Tilt positions

	Supine	30°	60 °	80 °	Standing
Phase shift (°)					
25th quantile	27.9°	29.3°	33.4°	34.3°	33.4°
Median	45.5°	42°	43.5°	40.6°	41.3°
75th quantile	54.3°	52.4°	49.5°	47.3°	42.5°
Deflection of RR (ms)					
25th quantile	144.1	158.9	138.8	127.7	100.4
Median	176.7	199.4	177.5	171.1	151.3
75th quantile	225.9	253.4	221.3	217.3	237.1
Deflection of P_S (mmHg)					
25th quantile	8.9	12.5	18.2	16.7	13.9
Median	9	13.5	20.5	19.5	17.9
75th quantile	10.4	16.3	23.4	22.2	23.4

Table 3.4: Phase shift and deflection of RR and P_S values.

The relationship between θ_0 and the BRS is illustrated in Figure 3·5. Although there is a difference of just 3° between the median orientation angles of supine(87.96°) and standing(84.91°), the high angle of the non-linear tangents function results in a BRS difference of 16.8 ms/mmHg between the median supine(28) and standing(11.2) values.

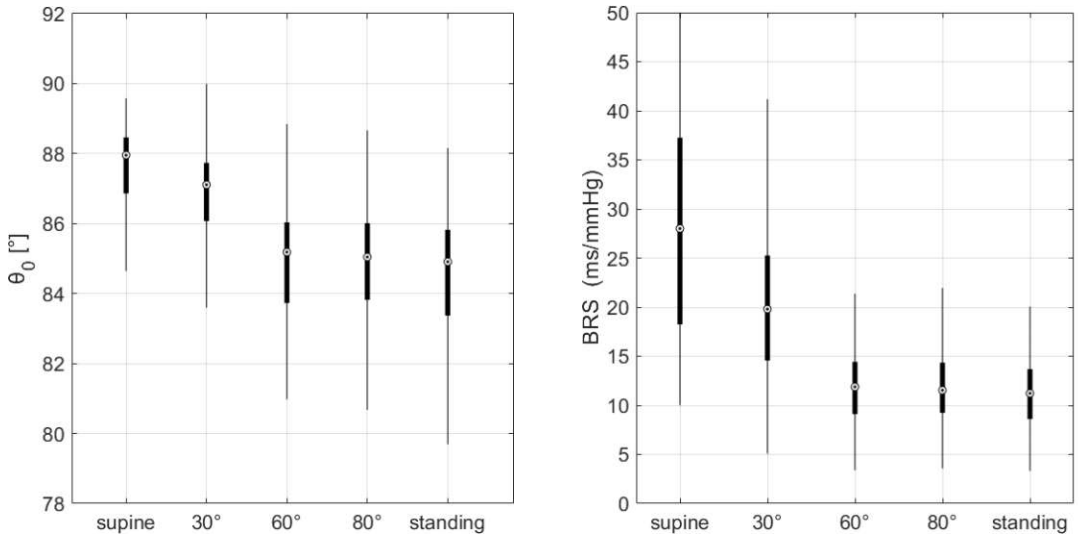

(a) Orientation angle θ_0 **(b)** BRS

Figure 3·5: In (a) the angles θ_0 of all ellipses for each position are depicted. With $BRS = \tan^{-1}\theta_0$ the BRS for ellipses is shown in (b) [1].

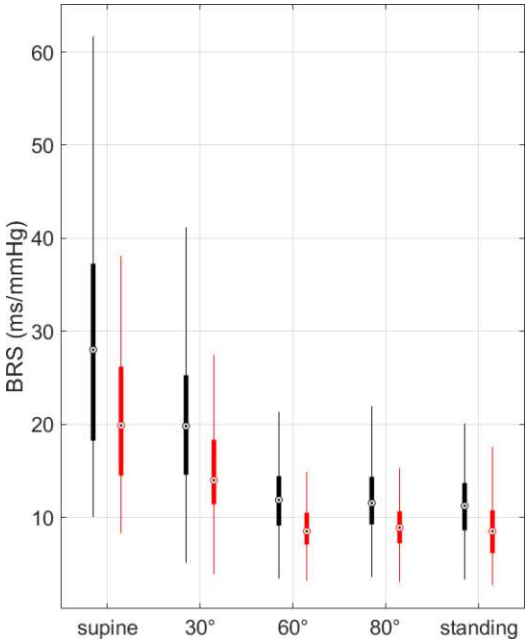

Figure 3·6: BRS of ellipse method(■) and regression(■)

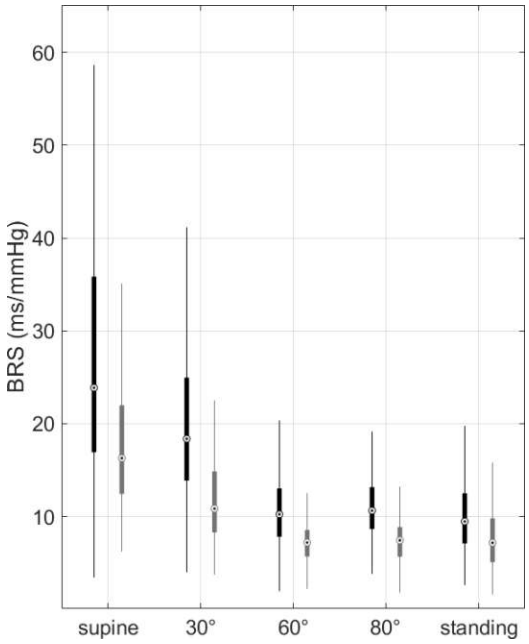

Figure 3·7: BRS of CBC up(■) and down-sequences(■).

Figure 3·6 compares the *BRS* estimate from the ellipse method to that produced by linear regression. The ellipse methods estimates are higher with values of 28, 19.8, 11.9, 11.5 and 11.2 ms/mmHg, whereas the regression results in estimates of 18.9, 14.5, 8.2, 8.8 and 8.6 ms/mmHg for the supine, 30°, 60°, 80° and standing position. The correlation between the two methods varies significantly, with coefficients of 0.76, 0.56, 0.77, 0.73 and 0.63 for supine, 30°, 60°, 80° and standing [2].

BRS estimates for the up-sequences of the CBCs are much higher than the down sequences, as shown in Figure 3·7. The median *BRS* estimates for up sequences using the ellipse method results in 26.8, 21.6, 11.8, 12.5 and 10.5 ms/mmHg over supine, 30°, 60°, 80° and standing, for down sequences 17.5, 11.8, 7.6, 7.7, 7.8 ms/mmHg. The same trend can also be seen for the regression method. The detailed values for the both the ellipse method and the regression are shown in Table A.2, with Table A.1 providing the number of sequences used in each measurement..

[1] the difference in both *BRS* and θ_0 between 60°-80°, 60°-standing and 80°-standing is not significant ($p < 0.05$)

[2] 2 outliers removed for the 30° and 1 outlier removed for supine

3.1.3 Beat to Beat Analysis

An analysis of up and down sequences that make up the spontaneous CBCs for the supine, 30°, 60°, 80° and standing position can be seen in Figures 3·8 and 3·9. The up sequences correspond to the expiration phase of the CBC, the down sequences to the inspiration. The beat to beat deflection of P_S (Figure 3·9, a) and RR (Figure 3·9, c) clearly illustrate a difference between the between the supine, 30° and the 60 °, 80°, standing positions. For the start of the up sequence, supine, and to a lesser degree 30° positions show decreased P_S change and increased RR change compared to the 60 °, 80°, standing group, indicating higher baroreflex efficiency. Over the whole sequence the mean deflection of P_S for the supine and 30° positions amount to a 2.1% and 3.1% change, the deflections for the 60 °, 80°, standing to a 3.7%, 3.3% and 3.2% change. The RR deflections over the whole sequence show the reverse trend, with a 5%, 5.4%, 4.5%, 4.5% and 4.4% change for supine, 30°, 60°, 80° tilt and standing, respectively.

This trend is also mirrored in the change in BRS (Figure 3·8), a decreasing amount of change from supine to 30° to 60° with virtually no change between 60°, 80° and standing. Also visible is the characteristic change in behaviour from inspiration to expiration, the P_S change during inspiration is elevated about 11.3%, whereas the RR change is reduced by 27.7%. A more detailed breakdown for each position is shown in Table A.3. It is interesting to note that the changes in BRS are inversely related to the change in P_S and directly related to the change in RR, a fact that can be directly observed in Figure 3·9. This shows the blood pressure regulating ability of the baroreflex, a decreased change in P_S at the expense of increased RR variability. All sequences had outliers above 3 standard deviations removed, due to extremely large outliers on some beat to beat changes in the BRS for the supine and 30° positions.

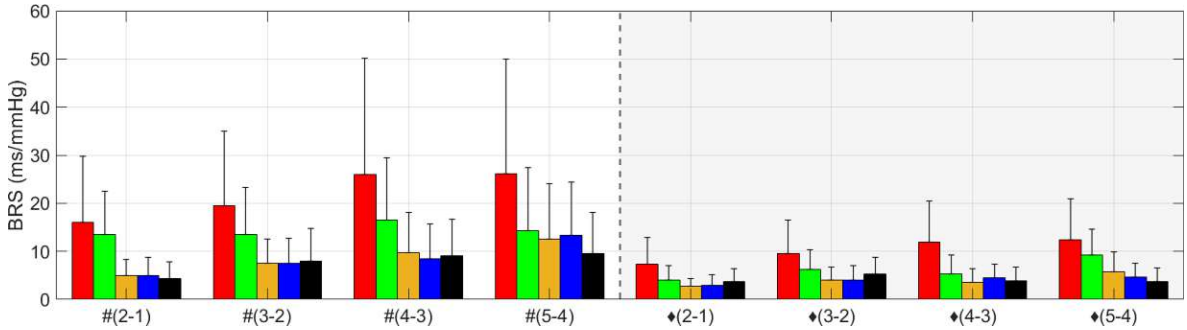

Figure 3·8: Beat to beat changes in BRS for the supine(■), 30°(■), 60°(■), 80°(■) and standing(■) positions. Up sequence to the left, down sequence right. Mean and standard deviation, outliers were removed.

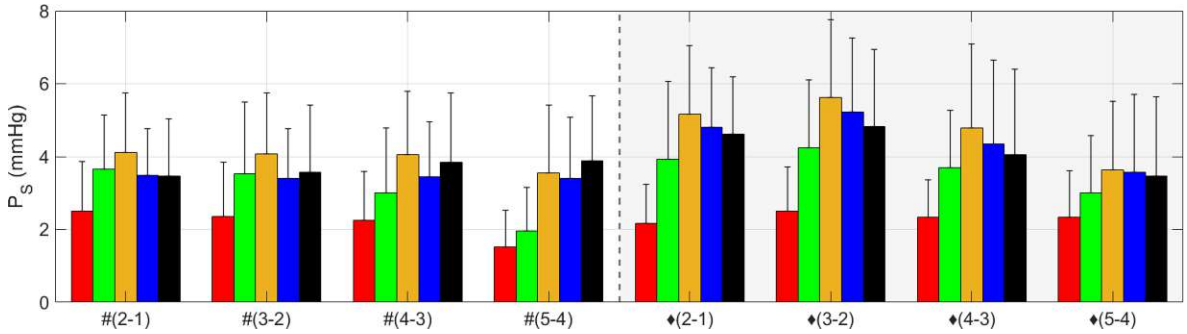

(a) Beat to Beat change P_S

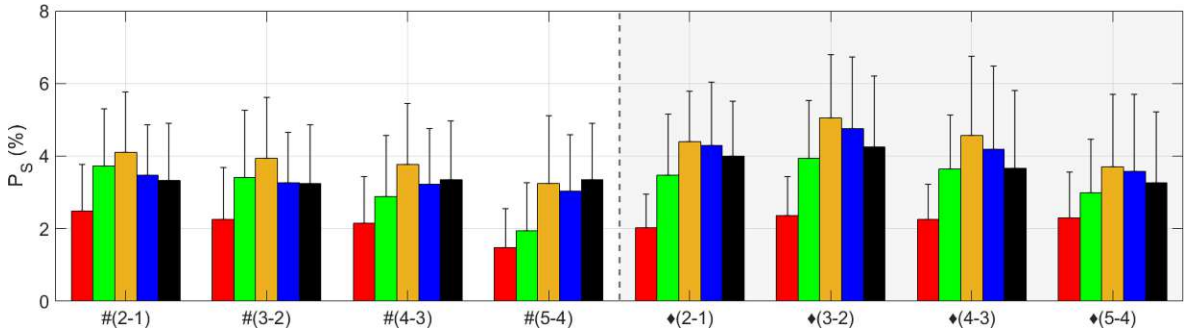

(b) Beat to Beat change normalised P_S

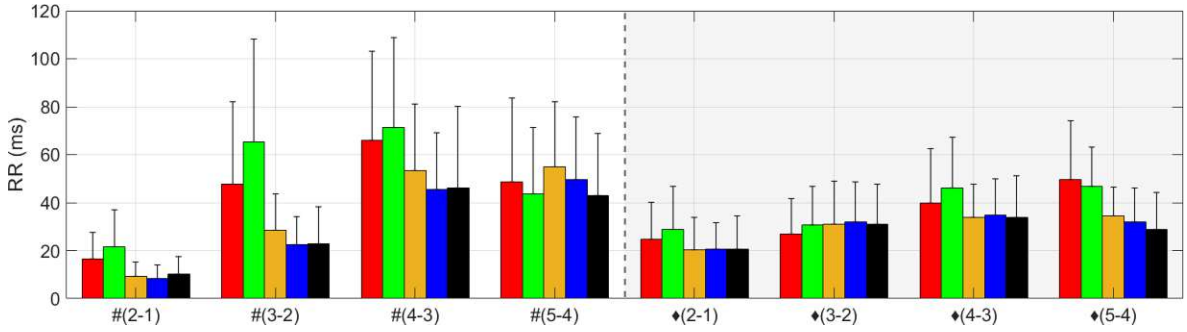

(c) Beat to Beat change RR

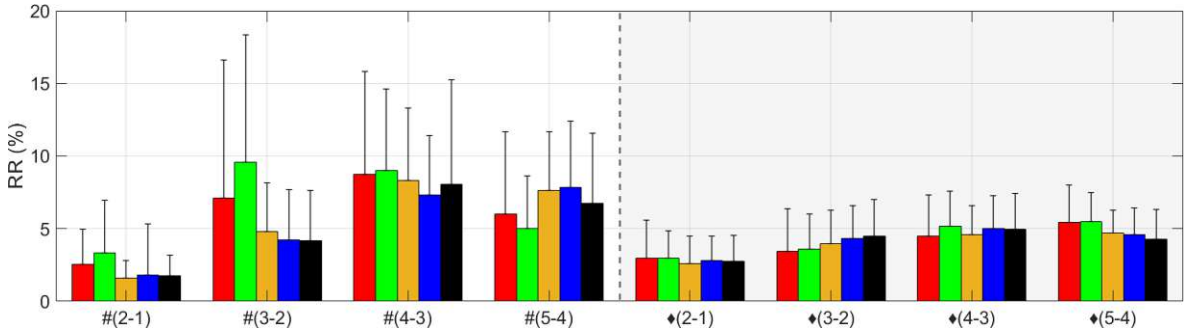

(d) Beat to Beat change normalised RR

Figure 3·9: The Beat to beat changes for the supine(■), 30°(■), 60°(■), 80°(■) and standing(■) positions. Up sequence to the left, down sequence right. Mean and standard deviation, outliers for P_S and RR were removed beforehand.

3.2 Vagus Nerve Stimulation

Here the results of the aVNS experiments are presented.

3.2.1 Validation of synchronised aVNS

To verify the synchronised stimulation was accurate each synchronisation signal was normalised, in time and value, with the cumulative stimulation percentage overlayed. This allows for a visual representation of the stimulation timing, with each experiment individually verified. Representative examples presented in Figures 3·10 and 3·11 show the stimulation distribution for both cardiac gated and respiratory gated experiments.
The cardiac gated aVNS additionally shows the blood pressure curve time shifted by 0.2 seconds (in black), showing the pressure curve at the approximate location of the heart. Although the stimulation signal slightly overlaps the systole and diastole boundary, it nevertheless shows a successful synchronisation.

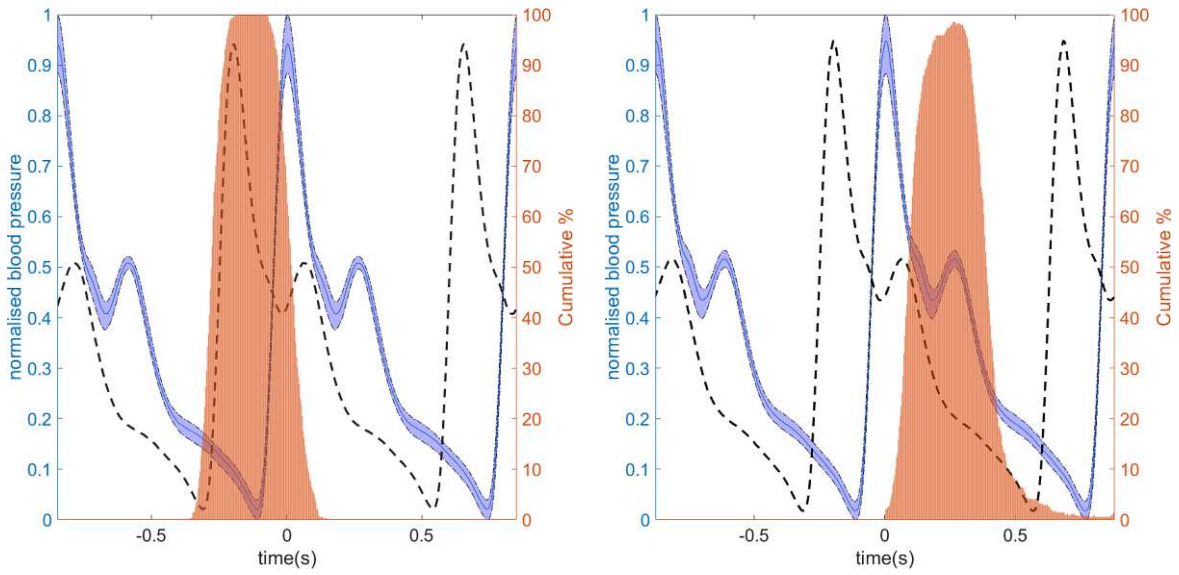

(a) Systolic synchronised aVNS **(b)** Diastolic synchronised aVNS

Figure 3·10: The cumulative cardiac gated stimulation signal(■) overlaid with the normalised blood pressure(■). The shaded area represents the 25%-75% IQR of the pressure curve. The additional striped curve(■) represents the 0.2s time shifted signal, and roughly represents the signal at time of stimulation.

The respiratory gated experiments exhibit a slight postponement in the onset of stimulation, mainly due to the processing delay of the stimulators' curve recognition. It is also notable that the stimulation usually terminates before the end of the respiration phase. This is most likely an artefact of the imperfect response of the respiration belt to the expansion and contraction of thoracic cavity. Nevertheless the respiration gated stimulation can also be considered successful.

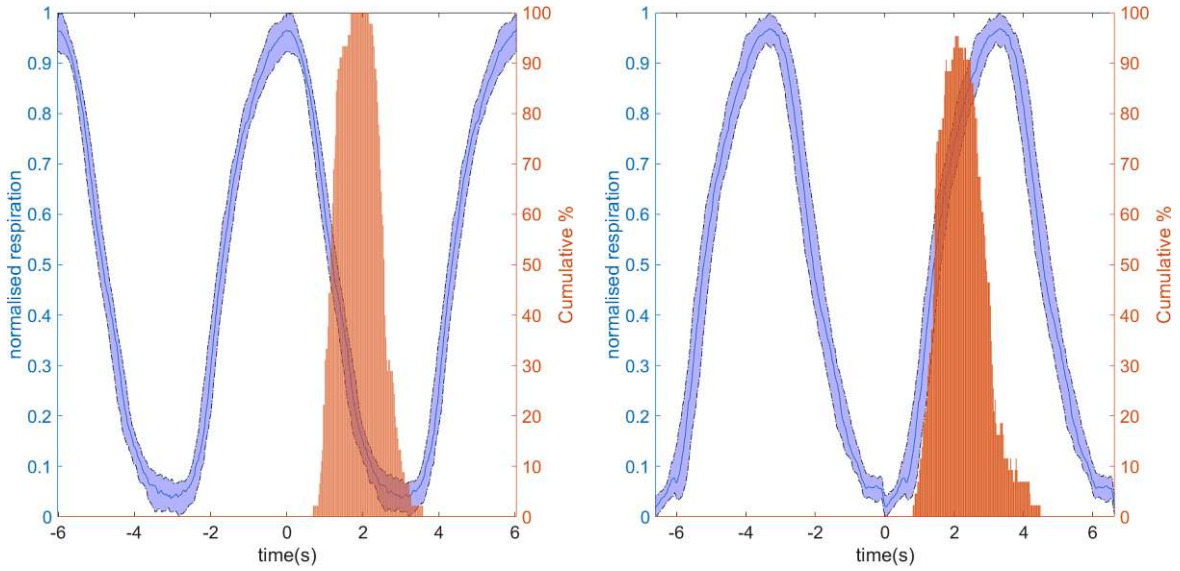

(a) Expiration synchronised aVNS **(b)** Inspiration synced aVNS

Figure 3·11: The cumulative respiration gated stimulation signal(■) overlaid with the normalised respiration(■). The shaded area represents the 25%-75% IQR of the respiration signal.

3.2.2 Synchronized aVNS

Both the cardiac gated aVNS and respiratory gated aVNS measurements were analysed for changes in P_S, P_D, *RR*, *LF*, *HF*, *RMSSD* and *SDNN*. For the cardiac gated aVNS experiment no statistically significant changes were observed between non-synchronised, diastolic synchronised and systolic synchronised aVNS. Furthermore no general trends for any of the values were observed. Nevertheless, for visualisation purposes lineplots were created, connecting the *RMSSD* and *SDNN* values for each measurement with each subject having a different colour. They are shown in shown in Figures 3·12 and 3·13.

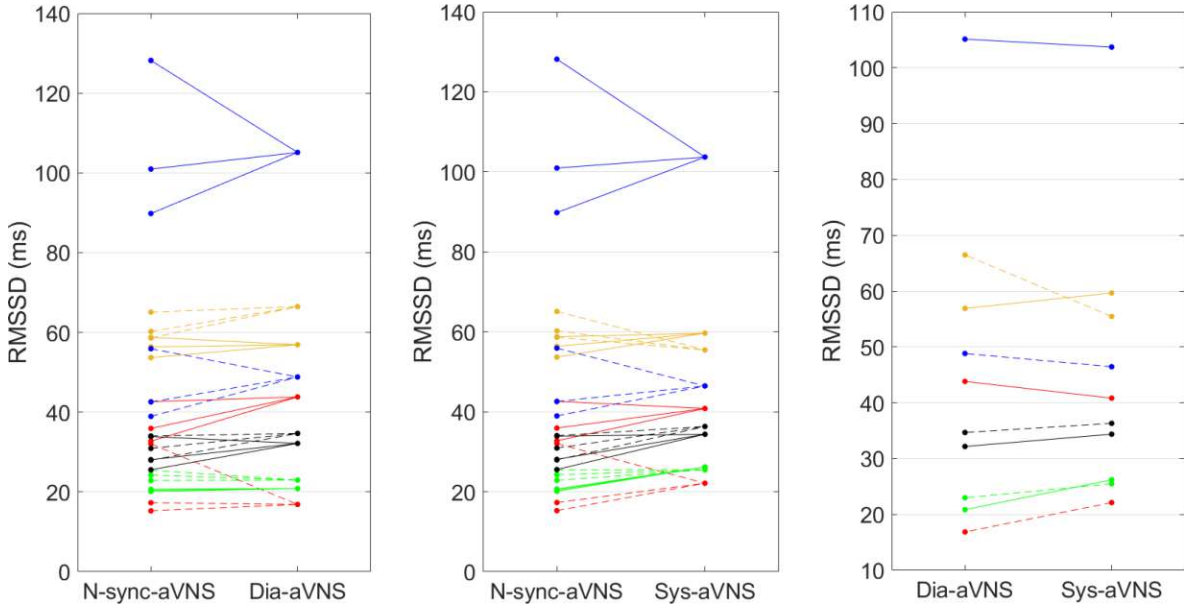

Figure 3·12: The trend in *RMSSD* between non synchronised aVNS, systolic synchronised aVNS, and diastolic synchronised aVNS. Subject colours are as follows, S1(■), S2(■), S3(■), S4(■) and S5(■). There are 3 recordings of the non synchronised aVNS, the second measurement for each subject is striped.

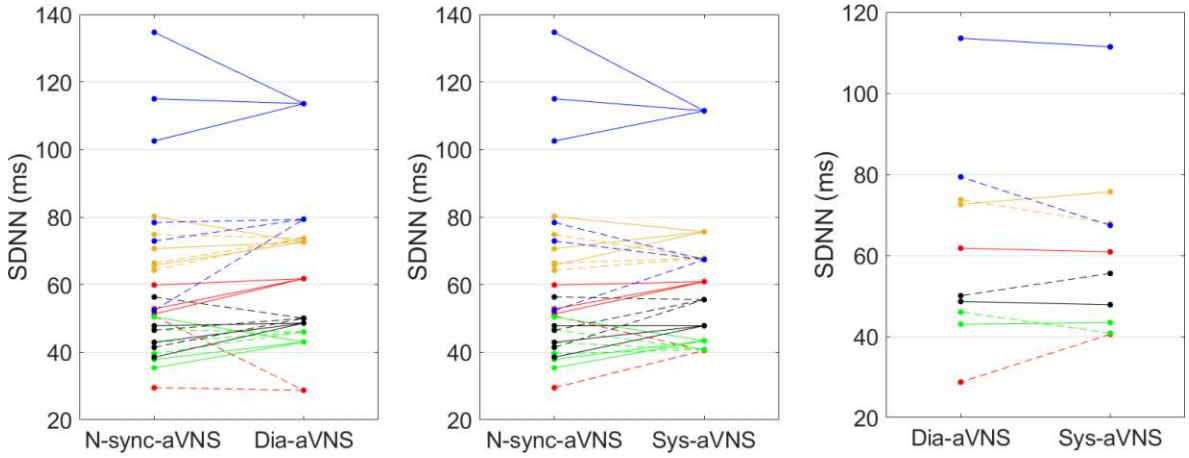

Figure 3·13: The trend in *SDNN* between non synchronised aVNS, systolic synchronised aVNS, and diastolic synchronised aVNS. Subject colours are as follows, S1(■), S2(■), S3(■), S4(■) and S5(■). There are 3 recordings of the non synchronised aVNS, the second measurement for each subject is striped.

A Radar plot depicting the median and IQR values for the P_S, P_D, *RR*, *LF*, *HF*, *RMSSD* and *SDNN* parameters for all cardiac and respiratory gated stimulation setting is shown Figure 3·16. There the large measurement to measurement variance within each stimulation protocol is clearly visible.

The respiratory gated experiments also did not show statistically significant changes in the P_S, P_D, *RR*, *LF*, *HF*, *RMSSD* and *SDNN* between non stimulation, inspiratory and expiratory gated aVNS. A significant decrease in the respiration rate was recorded between the non stimulation and the expiratory gated aVNS, with the inspiratory-gated aVNS showing a non-significant, although noticeable decrease as well. The respiration values are shown in Table 3.5. Furthermore an increasing trend was observed for the *RMSSD* values between non stimulation and the respiratory gated stimulation. Here a lineplot was also created, connecting the *RMSSD* values for each measurement with each subject having a different colour. It is shown in Figure 3·14. The same plot was also created for the *SDNN*, seen in Figure 3·15, although no trends were observed.

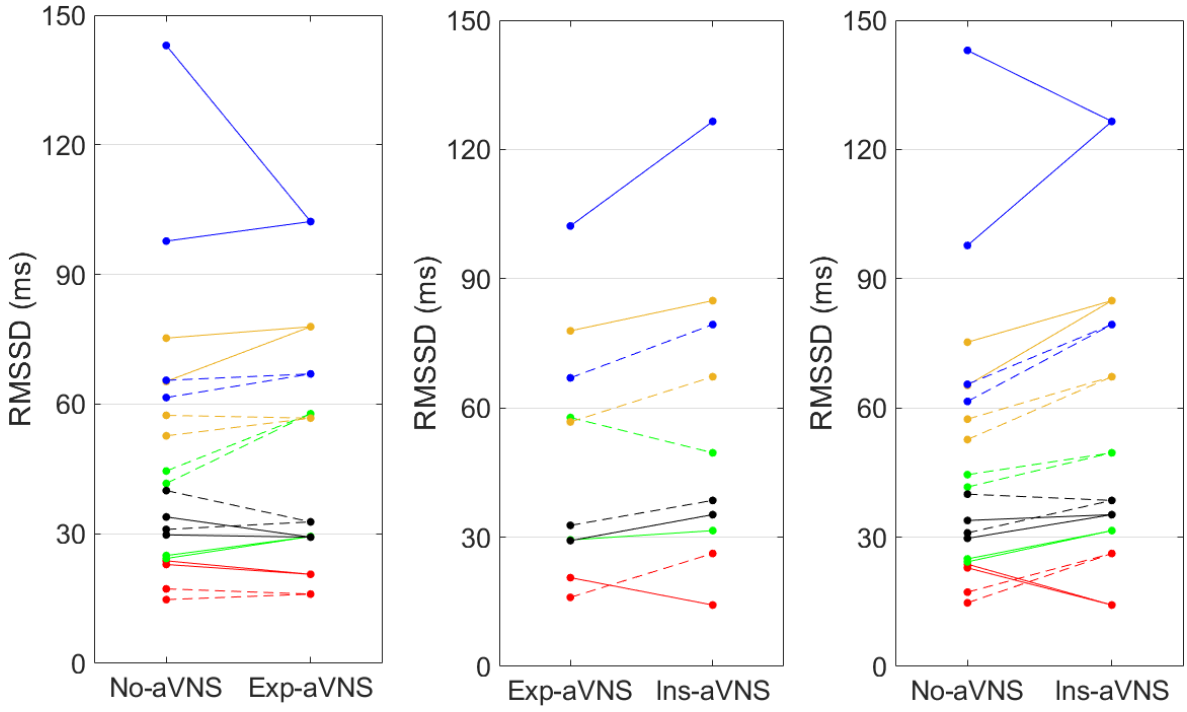

Figure 3·14: The trend in *RMSSD* between no-aVNS, expiratory synchronised aVNS, and inspiratory synchronised aVNS. Subject colours are as follows, S1(■), S2(■), S3(■), S4(■) and S5(■). The second measurement for each subject is striped.

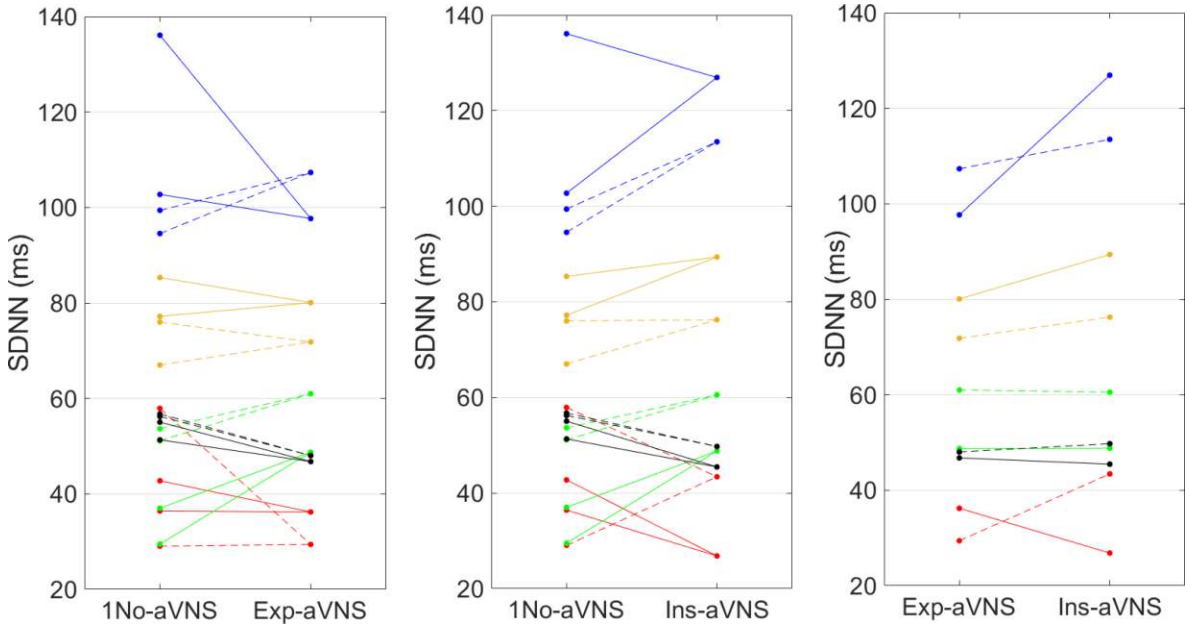

Figure 3·15: The trend in *SDNN* between no-aVNS, expiratory synchronised aVNS, and inspiratory synchronised aVNS. Subject colours are as follows, S1(■), S2(■), S3(■), S4(■) and S5(■). The second measurement for each subject is striped.

Stimulation Protocol	Respiration per minute
Non-sync. aVNS	16 (15.96 ± 4.62)
Systolic-sync. aVNS	15.11 (15.22 ± 4.64)
Diastolic-sync. aVNS	16.97 (16.61 ± 4.49)
No-aVNS	15.08 (15.24 ± 4.65)
Expiratory-synced aVNS	11.96 (13.13 ± 4.05)
Inspiratory-synced aVNS	13.82 (14.54 ± 4.41)

Table 3.5: Respirations per Minute, median (mean ± std)

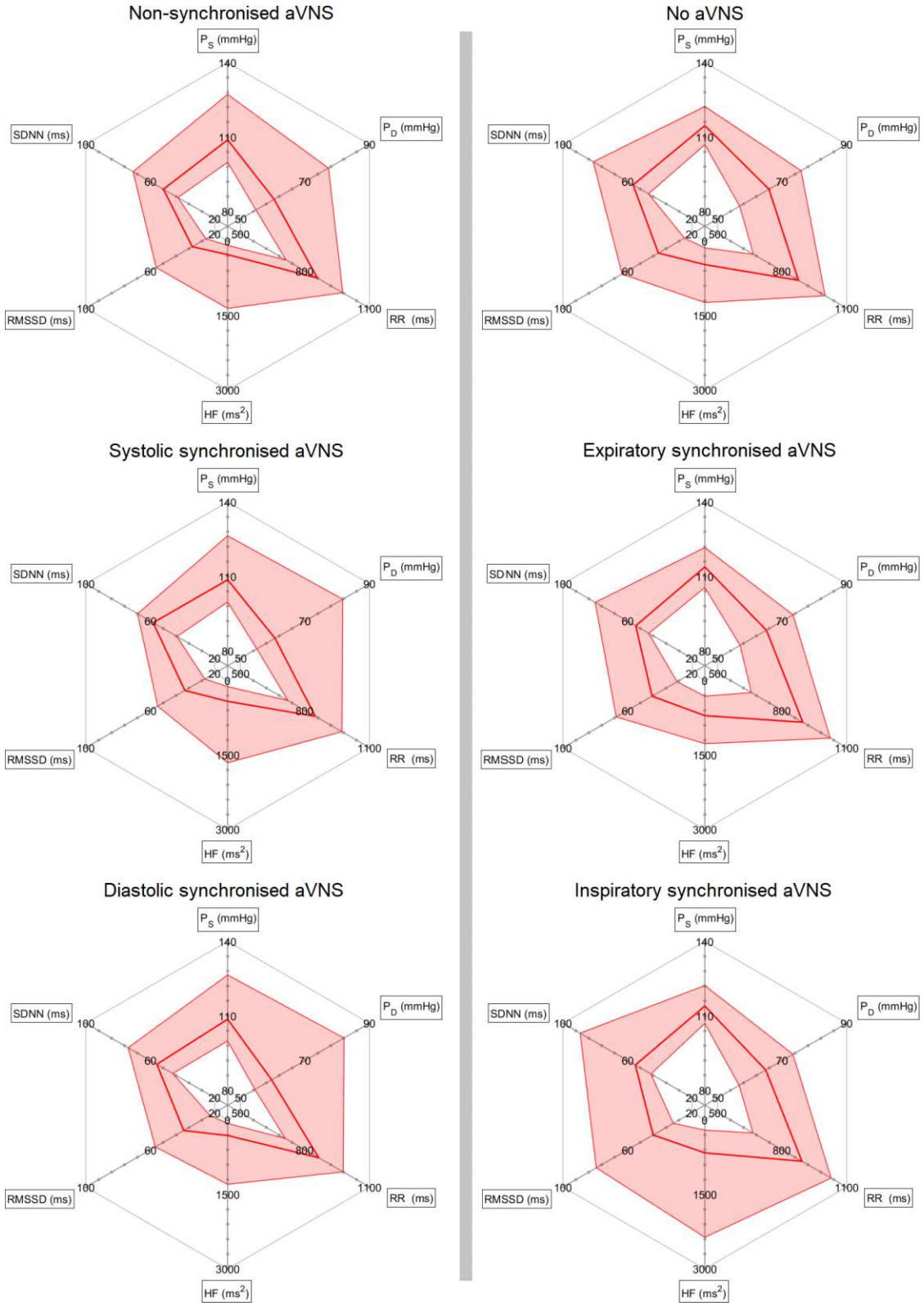

Figure 3·16: Radar plots with P_{S}, P_{D}, *RR*, *LF*, *HF*, *RMSSD* and *SDNN* for the different stimulations protocols. The median line is depicted bold red, the 25%-75% IQR as the shaded area.

Chapter 4

Discussion

This work conducted two separate experiments on the physiological response to external stimuli. Here the issues and implication of the results will be discussed.

4.1 Head-Up-Tilt Measurement

State of the art techniques to estimate *BRS* rely on spontaneous fluctuations of RR and P_S rather than induced changes through the us of drug infusion. This has the advantage of not only more closely reflecting the physiological behaviour of subject, but also allowing for longer, less time critical observations, simply because there are no drugs to wear of.(Milic et al., 2009) Slowed paced breathing is a simple method to increase spontaneous fluctuations and thereby aid the identification of baroreflex sequences.
An elliptic fit to model the baroreflex hysteresis has been proposed and recently implemented. This provides a reliable and potentially more accurate estimation for *BRS*.(Ler et al., 2010)

4.1.1 Ellipse Method

The best-fit ellipses' generated in this work show a clear pattern between the supine, 30°, 60°, 80° and standing positions. In Figure 3·2 it can be clearly seen that the median and IQR ellipses for the supine and 30° positions are both steeper and more elongated than the 60°, 80° and standing ellipses. In fact the 60°, 80° and standing ellipses are remarkably similar in shape and orientation, there being no significant difference in θ_0 between 60°-80°, 60°-standing and 80°-standing, and no significant difference in both major axis length a and minor axis length b between 60°-80° and 80°-standing.
The orientation angle decreases from the median standing ellipse angle of 88° to 87.1° for 30°, to 85.2°, 85°, 84.9° for the 60°, 80°, standing grouping. This results in a decrease in estimated *BRS* by 28%, 58%, 59% and 60% respectively. The lower sensitivity means that a change P_S results in a much smaller *RR* adjustment. It is also noticeable that the heart rate is significantly lower for supine and 30°, with the center *RR* value being 907ms and 873ms compared to 722 ms, 677 ms, 691 ms for 60°, 80° and standing.

It is hypothesised that the *BRS* reduction is due to a decrease in the neural component of the baroreflex(Taylor et al., 2013). In the more upright positions gravity causes blood to pool in the legs, reducing pressure in the upper body, deflating the barosensory vessels (e.g. aortic arch) and thereby reducing baroreceptor output. This leads to a decrease in PNS activity, a decrease in *BRS* and lowered *RR* variability. On the other hand PNS activity rises for more upright positions, leading to less linearity in the P_S-*RR* relationship, an increase in median P_D value and generally a wider hysteresis.(Cooke et al., 1999)
The supine and 30° ellipses median centers are also placed much higher than the 60°, 80° and standing, with an *RR* value of 907ms an 873ms compared to 722ms, 677ms and 691ms. The P_S median center also changes over the head up tilt, changing from 103mmHg to 103mmHg, 104mmHg, 109mmHg and 110mmHg over tilt from supine to standing. This once again shows higher blood pressure, but also heart rate for the upright positions, indicating that the supine and 30° positions exhibit a larger *BRS* for an equivalent change in heart rate.
Additional the ellipse method presents the time delay between the P_S and *RR*, seen in Figure 3·4, showing that throughout the ellipse, irrespective of upwards or downwards changes, the *RR* follows after the P_S. The median delay between *RR* and P_S decreases from 45.5° to 42°, 43,5°, 40,6° and 41,3° with increasing head-up tilt, indicating a higher baroreflex efficiency for the upright positions. It should be noted however, that there is a much greater range in delay between the supine IQR ellipses, 27.9° to 54.3°, than in the standing one, 33.4° to 42.5°, with only a small difference in median values. Previous experiments with paced breathing, although with 0.2 Hz instead of 0.1 Hz have displayed a much greater change, with a delay of 53° for 80° head up tilt, down to -12° for supine.(Cooke et al., 1999)(Karemaker and DeBoer, 2017) It is likely that this is an artefact of the slower paced breathing, or the ellipse method itself, that will be discussed later.

4.1.2 Regression

Figure 3·6, shows the estimated *BRS* for the ellipse method compared to the same calculated with a linear regression. The *BRS* calculated with the regression shows a mean decrease of 30%, 57%, 55% and 58% from supine to standing, compared to 28%, 58%, 59% and 60% for the ellipse method. Although absolute values for the regression are much lower, these results are remarkably similar and show the effectiveness of the ellipse method. The mean *BRS* for the regression, calculated for supine and standing shown in Table A.2, of (18.9 ms/mmHg) and(8.6 ms/mmHg), compare favourably with results obtained by (Laude et al., 2004b) of (13.0 ms/mmHg) and (6.7 ms/mmHg). The larger values estimated in this work are likely result of the increased baroreflex due to paced breathing.

4.1.3 Beat to beat

In Figure 3·9 the beat to beat changes in RR and P_S, separated into up and down sequences, corresponding to expiration and inspiration were shown. Here it is immediately obvious that the 60°, 80° and standing measurements exhibit the same grouping effect seen in the ellipse method. Also visible is the inverse relationship between P_S and RR seen when comparing supine and standing, showing the buffering effect of the baroreflex, sacrificing smaller heart rate variability for blood pressure stability. This trend can also be observed when looking at the BRS in Figure 3·8, with the supine position having the highest change in BRS, mirroring the small beat by beat change in P_S and the large difference in RR.
The large contrast in RR between the up (expiration) and down (inspiration) sequences could be explained by the fact that the baroreflex responds more strongly to the activation of baroreceptors due to increased P_S, leading to a stronger buffering response that slows the increase in P_S, but increases heart rate variability. The increased BRS during expiration seems to corroborate this theory (Studinger et al., 2007)(Kaniusas, 2012)(Incognito et al., 2020).

4.1.4 Limitations

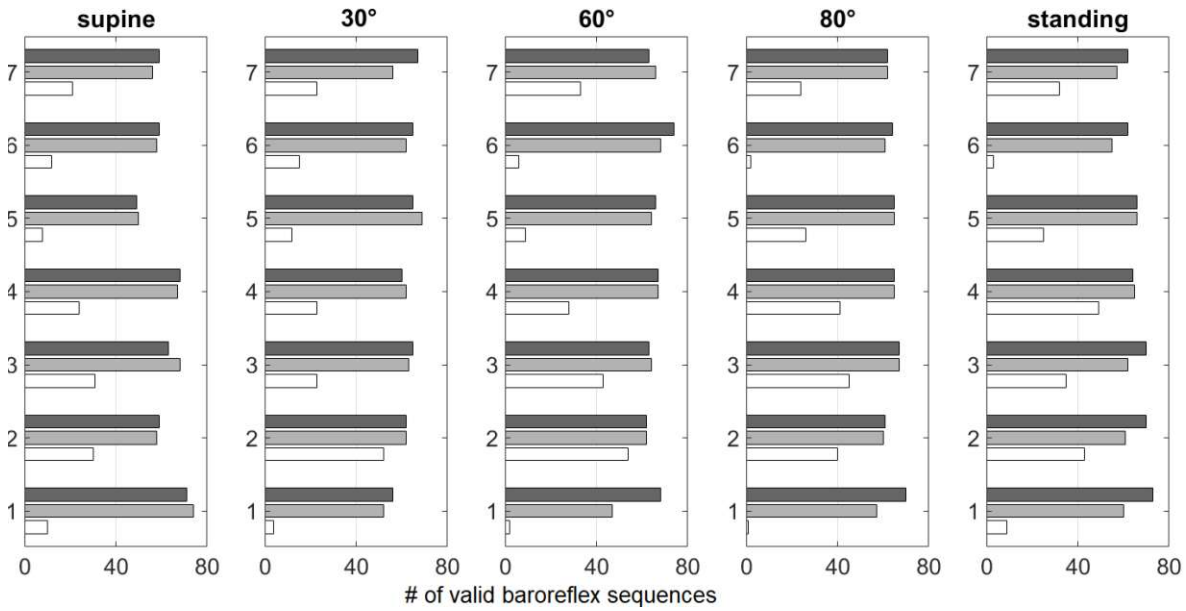

Figure 4·1: Number of down sequences(■), up sequences(■) and complete CBCs(□) for each subject.

Of the seven subjects only five contributed (2, 3, 4, 5, 7) contributed significantly to the up and down sequences that formed CBCs, with many sequences not long enough to form

a cycle. Nevertheless Figure 4·1 shows that, accounting for a slight variation in experiment length, a sequence was identified for most sequences. The compatibly low number of complete cycles likely stems from the strict correlation requirement of 0.85 between P_S and RR for a sequence to be considered valid, thereby shortening sequences to valid portions.
This issue of shortened sequences also appears to affect the CBCs. Measurements done using the Oxford method, where P_S is disturbed using intravenous drug injections, recorded a P_S deviation of ±15mmHg for supine and ±24mmHg for standing over the course of the measurement, which compares to ±13mmHg, ±11mmHg, ±15mmHg, ±15mmHg and ±14mmHg for supine, 30°, 60°, 80° and standing in the paced breathing experiment (Taylor et al., 2013) . Nevertheless, as shown in table 3.4 the median ellipse deflections of ±9mmHg (supine), ±13.5mmHg (30°), ±20.5mmHg (60°) ±19.5mmHg (80°) and ±17.9mmHg (standing) are smaller than what would be expected, considering the wider range of P_S values. Finally the mean CBC sequence length of 5 ± 1.1 beats is smaller than the expected number of 7.2 ± 1.3 beats based on the respiration rate, also suggesting incomplete cycles.

The limitations of the Vitalstream™ blood pressure cuff also played a part in the measurements. With a resolution of only 1mmHg and occasional dropouts resulting in missing heartbeat data the absolute blood pressure values should be considered carefully. Nevertheless, the device provides a stable long term average signal that, in practical application provides a more trustworthy offset than the Portapres® device.

4.2 Vagus Nerve Stimulation

Auricular vagus nerve stimulation is a novel therapy for the treatment of various chronic systematic disorders. Closed loop aVNS provides the ability to optimal adapt aVNS to each persons needs and allows for targeted synchronisation with a number of biosignals, such as ECG, PPG or Respiration(Dabiri1 et al., 2022).

4.2.1 Cardiac gated aVNS

Unfortunately no significant results were obtained for the cardiac gated aVNS. Vital and frequency parameters varied not only between subjects, but also within measurements of the same subject. It is likely that no results were observed because either the stimulation interval was too short, the subjects did not exhibit any pathologies for the aVNS to modulate, or a combination of those factors.

4.2.2 Respiratory gated aVNS

A previous experiment in expiration gated aVNS showed an increase in parasympathetic tone and cardiovagal activity, particularly *HF* power, *RMSSD* and *RR*, but no significant change in blood pressure(Staley et al., 2020). These experiments were conducted with patients suffering from hypertension, over multiple sessions lasting 30 minutes each. The measurements taken in this work were done on a much smaller time-frame of just 5 minutes and although no significant changes in cardiovagal activity were recorded, a trend of increasing *RMSSD*, indicating higher *HF* components, seen in Figure 3·14, was identified. Interestingly the change in *RMSSD* seems to be greater during inspiratory gated aVNS than expiratory gated aVNS. This could be because falling blood pressure during inspiration decreases PNS activity, which is then stimulated, whereas increasing blood pressure during expiration naturally increases PNS activity (Kaniusas, 2012).
A change in respiration frequency was also observed for the respiratory gated stimulation, shown in Table 3.5. Whether this is an artificial response due to subjects focusing in on stimulus, or a physiological response to the stimulation itself should be investigated further. It should also be noted that the change in respiration might mask or exaggerate trends in *RR*, *RMSSD* and *HF* components.

Chapter 5

Conclusion

Two separate experiments were preformed to investigate the cardiac response to a set of external stimuli. The variability in the heart rate has long been used as clinical indicator for various diseases and disorders, with recent attention being directed towards the baroreflex as an additional diagnostic tool. In the first part different head-up tilt positions were evaluated for spontaneous baroreflex sequences forming hysteresis during 0.1 Hz paced breathing exercises, to establish a set of reference values. The results were analysed for BRS using an ellipse fitted method and linear regression. The BRS values were calculated using the regression method compared well to BRS estimates from past studies. Furthermore the results of the ellipse method showed a moderate to strong correlation to the linear regression, with the ellipse estimates being higher than the regression.

A notable observation is the significant difference in BRS between the supine, 30° and 60° positions with the 60°, 80° and standing showing almost no difference between them. Future experiments could incorporate additional tilt positions at 15° and 45°, to more precisely investigate the region most sensitive to positional changes. Another discovery was the varying response of P_S to the tilt angles, in some subjects falling from supine, in others rising, the standing position nevertheless having the highest pressure. Similarly the size of the supine and 30° ellipses varied greatly between subjects, when compared to the 60°-80°-standing group. It remains to be seen if this is an artefact of the CBC selection criteria or natural variation between subjects.

For a future analysis it would be wise to compare ellipse method results using CBCs obtained with the 0.85 correlation requirement between P_S and RR and complete CBCs using all the available data. Nevertheless, with further refinement the ellipse method could very well become a widely used tool to estimate and visualise BRS for research purposes. Overall the experiment gave new insight into the response of BRS in different head-up tilt positions, validated the hysteresis behaviour of the baroreflex and investigated the ellipse method as new way to analyse and quantify the arterial barorflex.

For the second part additional experiments using cardiac and respiratory gated aVNS were performed. Here the performance of a new prototype aVN stimulator was evaluated and found satisfactory. Unfortunately the cardiac gated stimulation measurement did not yield any significant results. It is likely that either the stimulation duration of 5 minutes per session was too short or that possible modulating effects do not appear in healthy subjects. The respiratory gated stimulation however did show trends of increased PNS activity similar to results obtained in a previous study by other authors using longer stimulation sessions.

In conclusion the experiments can be considered a success in demonstrating the utility of the prototype aVN stimulator. For future amassments of synchronised aVNS a more focused approach in choosing subjects and stimulation duration seems necessary, with respiratory gated aVNS so far showing promise for further investigations.

It is highly likely that synchronised aVNS will one day have clinical application in the personalised treatment of various disorders and diseases. Already portable aVNS devices are being developed and slowly brought to market, it seems only a matter of time before biofeedback-based aVN stimulators will become available. Even so, research is still in it's infancy and it remains to be seen how much of an improvement closed loop aVNS offer over non synchronised aVNS.

Appendix A

Annex

	Supine	30°	60°	80°	standing
E_{up}	417	421	431	426	415
E_{dn}	415	427	460	444	459
E_{all}	832	848	891	870	874
R_{up}	362	375	393	402	401
R_{dn}	422	433	458	438	452
R_{all}	784	808	851	840	853
$E_{up,\ CBC}$	131	151	174	176	194
$E_{dn,\ CBC}$	132	150	175	179	195
$E_{all,\ CBC}$	263	301	349	355	389
$R_{up,\ CBC}$	136	152	175	179	196
$R_{dn,\ CBC}$	136	152	175	179	196
$R_{all,\ CBC}$	272	304	350	358	392
CBC	136	152	175	179	196

Table A.1: Number of valid sequences for each tilt position, see Table A.2

	Supine	30°	60°	80°	standing
E $_{up}$	23.6 (28.7 ± 22.3)	20.3 (22.5 ± 14)	11.7 (12.7 ± 7.1)	11.6 (12.1 ± 6.9)	10.1 (11.4 ± 6.5)
E $_{dn}$	18 (20.7 ± 12.4)	12.3 (14.7 ± 9.4)	7.6 (8.8 ± 5.7)	7.7 (8.4 ± 5.1)	7.4 (8.4 ± 5.1)
E $_{all}$	19.9 (24.7 ± 18.5)	15.9 (18.6 ± 12.6)	9.1 (10.7 ± 6.7)	9 (10.2 ± 6.3)	8.7 (9.8 ± 6)
R $_{up}$	19.8 (24.4 ± 20)	17.3 (19 ± 12)	10.1 (10.9 ± 7.2)	9.9 (11.4 ± 17.7)	9.1 (9.5 ± 4.4)
R $_{dn}$	16.7 (19 ± 10.8)	11.3 (14.2 ± 11.4)	7.3 (8.1 ± 4.7)	7.2 (7.8 ± 5)	6.7 (8 ± 12.9)
R $_{all}$	17.8 (21.5 ± 15.9)	14.3 (16.4 ± 11.9)	8.3 (9.4 ± 6.1)	8.3 (9.5 ± 12.9)	8 (8.7 ± 9.9)
E $_{up, C}$	26.8 (35.2 ± 29.7)	21.6 (24.8 ± 15.2)	11.8 (12.3 ± 5.7)	12.5 (12.9 ± 5.1)	10.5 (11.6 ± 5.2)
E $_{dn, C}$	17.5 (20 ± 11.6)	11.8 (13.5 ± 7.2)	7.6 (8 ± 2.9)	7.7 (8.2 ± 3.5)	7.8 (8.4 ± 4.5)
E $_{all, C}$	21.2 (27.6 ± 23.7)	16.2 (19.2 ± 13.2)	8.9 (10.2 ± 5)	9.4 (10.5 ± 4.9)	9.2 (10 ± 5.1)
R $_{up, C}$	23.9 (30.9 ± 25.7)	18.4 (21.6 ± 13.2)	10.3 (11.2 ± 7.9)	10.6 (13.3 ± 25.2)	9.5 (10.1 ± 4)
R $_{dn, C}$	16.3 (18.5 ± 10.2)	10.9 (12.3 ± 6.6)	7.2 (7.3 ± 2.3)	7.4 (7.5 ± 3)	7.2 (7.7 ± 3.7)
R $_{all, C}$	18.9 (24.7 ± 20.5)	14.5 (17 ± 11.4)	8.2 (9.3 ± 6.1)	8.8 (10.4 ± 18.2)	8.6 (8.9 ± 4.1)
CBC [3]	28 (31.3 ± 19.5)	19.8 (22.2 ± 12.9)	11.9 (12.2 ± 5.1)	11.5 (11.5 ± 12.5)	11.2 (12.2 ± 11.5)

Table A.2: *BRS* (ms/mmHg) for all sequences for each position. The Ellipse method is shown as E, Regression as R. The C denotes sequences compromising a CBC, with all estimates being made with either up or down sequences and only the CBC estimate using the complete up and down cycles. Median (Mean ± Dtd).

[3] 2 outliers removed for the 30° position and 1 outlier removed for 80°

	Supine	30°	60°	80°	standing
$P_{S,\ up}$	2.17 ± 1.38	2.98 ± 1.81	3.63 ± 1.85	3.2 ± 1.53	3.45 ± 1.85
$RR_{\ up}$	42.7 ± 35.4	48.1 ± 38.2	34.8 ± 26.7	31.3 ± 23.8	30.2 ± 25.3
$BRS_{\ up}$	20.34 ± 19.35	14.53 ± 11.45	8.91 ± 8.72	8.78 ± 8.26	7.75 ± 7.47
$P_{S,\ dn}$	2.2 ± 1.18	3.5 ± 1.91	4.12 ± 2.35	3.84 ± 2.24	3.59 ± 2.2
$RR_{\ dn}$	34.3 ± 21.6	38 ± 19.5	28.5 ± 14.7	27 ± 14.5	25.1 ± 15.4
$BRS_{\ dn}$	10.02 ± 9.12	6.92 ± 14.1	4.51 ± 6.52	4.53 ± 4.65	4.78 ± 4.74
$P_{S,\ all}$	2.19 ± 1.27	3.26 ± 1.88	3.89 ± 2.14	3.53 ± 1.95	3.52 ± 2.05
$RR_{\ all}$	38.1 ± 29	42.6 ± 30.1	31.5 ± 21.5	29.1 ± 19.6	27.5 ± 20.7
$BRS_{\ all}$	14.51 ± 15.36	10.38 ± 13.5	6.59 ± 7.94	6.63 ± 7	6.15 ± 6.33

Table A.3: Beat to beat changes P_S (mmHg), RR (ms) and BRS (ms/mmHg) for up, down and all sequences over each Head Up-Tilt position. The values are averaged over the whole length of each sequence. (Mean ± std).

References

Badran, B. W. et al. (2018). Short trains of transcutaneous auricular vagus nerve stimulation n (tavns) have parameter-specifc effects on heart rate. *Brain Stimulation*, 11(4).

Baruch, M. C. et al. (2011). Pulse decomposition analysis of the digital arterial pulse during hemorrhage simulation. *Nonlinear Biomedical Physics*, 5:Article 1.

Ben-Menachem, E. (2000). Vagus-nerve stimulation for the treatment of epilepsy. *The Lancet Neurology*, 1(8):477–482.

Benarroch, E. E. (2008). The arterial baroreflex: functional organization and involvement in neurologic disease. *Neurology*, 71:1733–1738.

Bermejo, P. et al. (2017). Innervation of the human cavum conchae and auditory canal: Anatomical basis for transcutaneous auricular nerve stimulation. *BioMed Research International*, vol. 2017:10 pages.

Berthoud, H. R. and Neuhuber, W. L. (2000). Functional and chemical anatomy of the afferent vagal system. *Auton. Neurosci.*, 85:1–17.

Bilgeand, A. R., Stein, P. K., Domitrovich, P. P., et al. (1999). Assessment of ultra low frequency band power of heart rate variability: validation of alternative methods. *International Journal of Cardiology*, 71:1–6.

BIOPAC Systems Inc. *BSL Hardware Guide*. BIOPAC Systems Inc.

Caretaker Medical. Vitalstream product description. https://caretakermedical.net/continuous-vital-monitoring/. 2022-10-15.

Chapleau, M. W. (2012). *Baroreceptor reflexes*, chapter 33, pages 161–165. Academic Press.

Choi, Y., Ko, S., and Ying, S. (2006). Effect of postural changes on baroreflex sensitivity: A study on the eurobavar data set. *2006 Canadian Conference on Electrical and Computer Engineering*, 1:110–114.

Clancy, J. A., Deuchars, S. A., and Deuchars, J. (2012). The wonders of the wanderer. *Exp. Physiol*, 98:38–45.

Cook, D. N. et al. (2020). Design and validation of a closed-loop, motor-activated auricular vagus nerve stimulation (maavns) system for neurorehabilitation. *Brain Stimulation*, 13(3):800–803.

Cooke, W. H., Hoag, J. B., Crossman, A. A., Kuusela, T. A., Tahvanainen, K. U., and Eckberg, D. L. (1999). Human responses to upright tilt: a window on central autonomic integration. *J. Physiol*, 517:617–628.

Dabiri, B., Brito, J., and Kaniusas, E. (2021). Cardiovagal baroreflex hysteresis using ellipses in response to postural changes. *Front. Neurosci.*, 15.

Dabiri1, B., Zeiner, K., Nativel, A., and Kaniusas, E. (2022). Auricular vagus nerve stimulator for closed-loop biofeedback-based operation. *Analog Integrated Circuits and Signal Processing*, 112:237–246.

Eckberg, D. L. and Sleight, P. (1992). Human baroreflexes in health and disease. *Oxford: Clarendon Press*.

Eckert, S. and Horstkotte, D. (2001). Comparison of portapres non-invasive blood pressure measurement in the finger with intra-aortic pressure measurement during incremental bicycle exercise. *Blood pressure Monitoring*, 7(3):179–183.

E.Hein, Nowak, M., Kiess, O., Biermann, T., K.Bayerlein, Kornhuber, J., et al. (2012). Auricular transcutaneous electrical nerve stimulation in depressed patients: a randomized controlled pilot study. *J. Neural Transm.*, 120:821–827.

Hart, E. C., Wallin, B. G., Curry, T. B., et al. (2011). Hysteresis in the sympathetic baroreflex: role of baseline nerve activity. *J Physiol*, 589:3395–3404.

Hughson, R. L., Quintin, L., Annat, G., Yamamoto, Y., and Gharib, C. (1993). Spontaneous baroreflex by sequence and power spectral methods in humans. *Clinical Physiology*, 13:663–676.

Incognito, A. V., Samora, M., Shepherd, A. D., et al. (2020). Sympathetic arterial baroreflex hysteresis in humans: different patterns during low- and high-pressure levels. *Am J Physiol*, 319:787–792.

Kaniusas, E. (2012). *Biomedical Signals and Sensors I*. Springer, Berlin, Heidelberg.

Kaniusas, E. et al. (2020). Stimulation pattern efciency in percutaneous auricular vagus nerve stimulation: Experimental versus numerical data. *IEEE transactions on bio-medical engineeringl*, 67(7):1921–1935.

Kaniusas, E., Kampusch, S., Tittgemeyer, M., Panetsos, F., Gines, R. F., Papa, M., Kiss, A., Podesser, B., Cassara, A., et al. (2019a). Current directions in the auricular vagus nerve stimulation i – a physiological perspective. *Front. Neurosci.*, 13:854.

Kaniusas, E., Kampusch, S., Tittgemeyer, M., Panetsos, F., Gines, R. F., Papa, M., Kiss, A., Podesser, B., Cassara, A. M., Tanghe, E., Samoudi, A. M., Tarnaud, T., Joseph, W., Marozas, V., Lukosevicius, A., Ištuk, N., Lechner, S., Klonowski, W., Varoneckas, G., Széles, J. C., and Šarolić, A. (2019b). Current directions in the auricular vagus nerve stimulation ii – an engineering perspective. *Frontiers in Neuroscience*, 13.

Karemaker, J. and DeBoer, R. (2017). Vagal baroreflex latency in circulatorycontrol: letters. *J. Physiol*, 595:2197–2198.

Kumar, P. and Yildirim, E. A. (2005). Minimum-volume enclosing ellipsoids andcore sets. *J. Optim. Theory Appl.*, 126:1–21.

LaRovere, M. T. et al. (1998). Baroreflex sensitivity and heart-rate variability in prediction of total cardiac mortality after myocardial infarction. atrami (autonomic tone and reflexes after myocardial infarction) investigators. *Lancet,*, 351:478–484.

Laude, D. et al. (2004a). Comparison of various techniques used to estimate spontaneous baroreflex sensitivity (the eurobavar study). *Am J Physiol Regul Integr Comp Physiol*, 286:226–231.

Laude, D. et al. (2004b). Comparison of various techniques used to estimate spontaneous baroreflex sensitivity (the eurobavar study). *Am J Physiol Regul Integr Comp Physiol*, 286:226–231.

Ler, A. S., Cohen, M. A., and Taylor, J. A. (2010). A planar elliptical model of cardio-vagal hysteresis. *Am J Physiol*, 276:1691–1698.

Lowry, M., Windsorand, J., and Ashelford, S. (2016). Orthostatic hypotension 2: the physiology of blood pressure regulation. *Nursing Times*, 112:17–19.

Malmivuo, J. and Plonsey, R. (1995). *Bioelectromagnetism - Principles and Applications of Bioelectric and Biomagnetic Fields.* Oxford University Press, New York.

Mercante, B., Ginatempo, F., Manca, A., Melis, F., Enrico, P., and Deriu, F. (2018). Anatomo-physiologic basis for auricular stimulation. *Med. Acupunct.*, 30:141–150.

Milic, M., Sun, P., Liu, F., Fainman, C., et al. (2009). A comparison of pharmacologic and spontaneous baroreflex methods in aging and hypertension. *Journal of hypertension*, 27:1243–1251.

Napadow, V. et al. (2012). Evoked pain analgesia in chronic pelvic pain patients using respiratory-gated auricular vagal aferent nerve stimulation. *Pain Medicine*, 13(6):777–789.

O'Leary, D. D., Kimmerly, D. S., Cechetto, A. D., and Shoemaker, J. K. (2003). Differential effect of head-up tilt on cardiovagal and sympathetic baroreflex sensitivity in humans. *Experimental Physiology*, 88:769–774.

Pagaduan, J., Wu, S. S., Kameneva, T., and Lambert, E. (2019). Acute effects of resonance frequency breathing on cardiovascular regulation. *Physiological Reports*, 7 (22):e14295.

Porter, B. A., Khodaparast, N., Fayyaz, T., Cheung, R. J., Ahmed, S. S., Vrana, W. A., et al. (2011). Repeatedly pairing vagus nerve stimulation with a movement reorganizes primary motor cortex. *Cereb. Cortex*, 22:2365–2374.

Raczak, G. et al. (2004). Arterial baroreflex modulation of heart rate in patients early after heart transplantation: lack of parasympathetic reinnervation. *Clinical Heart Transplantations*, pages 399–406.

Rea, R. F. and Eckberg, D. L. (1987). Carotid baroreceptor-muscle sympathetic relation in humans. *The American Journal of Physiology*, 6:929–934.

Rudas, L. et al. (1999a). Human sympathetic and vagal baroreflex responses to sequential nitroprusside and phenylephrine. *Am J Physiol*, 376:1691–1698.

Rudas, L. et al. (1999b). Human sympathetic and vagal baroreflex responses to sequential nitroprusside and phenylephrine. *Physiol Meas*, 31:857–873.

Sackeim, H. A. et al. (2005). Vagus nerve stimulation (vns™) for treatment-resistant depression: Efficacy, side effects, and predictors of outcome. *Neuropsychopharmacology*, 25(5):713–728.

S.Bauer, H.Baier, Baumgartner, C., Bohlmann, K., S.Fauser, W.Graf, et al. (2016). Transcutaneous vagus nerve stimulation (tvns) for treatment of drug-resistant epilepsy: a randomized, double-blind clinical trial (cmpse02)l. *Brain Stimul.*, 9:356–363.

Schweitzer, P. and Teichholz, L. E. (1985). Carotid sinus massage. its diagnostic and therapeutic value in arrhythmias. *Am. J. Med.l*, 78:645–654.

Shaffer, F. and Ginsberg, J. P. (2017). An overview of heart rate variability metrics and norms. *Front Public Health*, 15:258.

Staley, R., Garcia, R. G., l J. Stowel, et al. (2020). Modulatory effects of respiratory-gated auricular vagal nerve stimulation on cardiovagal activity in hypertension. *Proceedings of the annual international conference of the IEEE Engineering in Medicine and Biology Society, EMBS. Institute of Electrical and Electronics Engineers Inc*, page 2581–2584.

Stroobandt, R. X., Barold, S. S., and Sinnaeve, A. F. (2016). *ECG from Basics to Essentials:*. John Wiley & Sons.

Studinger, P., Goldstein, R., and Taylor, J. A. (2007). Mechanical and neural contributions to hysteresis in the cardiac vagal limb of the arterial baroreflex. *J Physiol*, 583:1041–1048.

Task Force of The European Society of Cardiology and The North American Society of Pacing and Electrophysiology (1997). Heart rate variability: Standards of measurement, physiological interpretation, and clinical use. *European Heart Journal*, 17:354–381.

Taylor, C. E., Willie, C. K., Atkinson, G., Jones, H., and Tzeng, Y. C. (2013). Postural influences on the mechanical and neural components of the cardiovagal baroreflex. *Acta Physiol (Oxf)*, 208:66–73.

Thayer, J. F., Yamamoto, S. S., and Brosschot, J. F. (2009). The relationship of autonomic imbalance, heart rate variability and cardiovascular disease risk factors. *Int. J. Cardiol*, 141:122–131.

Trepel, M. (2017). *Fundamental Principles of Optical Lithography*. Munich: Urban & Fischer.

van Schelvena, L. J., Karemakerd, J. M., Blankestijnb, P. J., and Oey, P. L. (2008). Short-term sympathetic baroreflex sensitivity increases at lower blood pressures. *Clinical Neurophysiology*, 119:869–879.

Williams, E. K., Chang, R. B., Strochlic, D. E., Umans, B. D., Lowell, B. B., and Liberles, S. D. (2016). Sensory neurons that detect stretch and nutrients in the digestive system. *Cell*, 166:209–221.

Zulfiqar, U., Jurivich, D. A., Gao, W., and Singer, D. H. (2010). Relation of high heart rate variability to healthy longevity. *Am. J. Cardiol*, 105:1181–1185.